INL-RPT-22-66979
Revision 0

Forecasted Dynamic Line Ratings for Regional Transmission Lines

June 2022

Alexander Abboud
Jacob Lehmer
Jake Gentle

Changing the World's Energy Future

Idaho National Laboratory

INL is a U.S. Department of Energy National Laboratory operated by Battelle Energy Alliance, LLC

INL-RPT-22-66979
Revision 0

Forecasted Dynamic Line Ratings for Regional Transmission Lines

Alexander Abboud
Jacob Lehmer
Jake Gentle

June 2022

Idaho National Laboratory
Idaho Falls, Idaho 83415

http://www.inl.gov

Prepared for the
U.S. Department of Energy
Wind Energy Technologies Office
Under DOE Idaho Operations Office
Contract DE-AC07-05ID14517

Page intentionally left blank

SUMMARY

This report was prepared for the Wind Energy Technology Office for the FY 2022, quarter 3 deliverable. This details the use of forecasted dynamic line rating as an improvement over static rating for three transmission lines in three regions of interest. A selection of wind plants across Idaho, the Columbia River Gorge and offshore wind in the NYSERDA territory were modeled for their concurrent cooling effects for dynamic line rating. Regional transmission lines for the wind plant interconnections were determined and a CFD domain was created to determine local wind flows over the lines. A dynamic line rating for each of the lines was calculated for both weather observation data and HRRR model forecast data. The comparison of peaks in the wind power production were compared to the DLR peaks.

It was determined that for shorter regional transmission lines, the benefits of concurrent cooling that commonly occur with gen-tie lines were still valid, that is there is a strong correlation with wind farm power generation and high dynamic line ratings. Concurrent cooling effects drop as the length of the regional transmission lines increase in distance from the wind plants. In addition, the accuracy of the forecasted ampacity to the weather observation data for ampacity was assessed. In general, the accuracy was best for the INL region with the NOAA-maintained sites. The Columbia River Gorge and Long Island sites showed similar levels of accuracy for the forecasted DLR. The accuracy levels were around 11% for the INL region, 15% for Columbia River Gorge and 7% for New York Long Island. The higher error for the Columbia Gorge region is likely due to the sparse availability of weather stations available, whereas both the INL site and Long Island are well instrumented.

Page intentionally left blank

CONTENTS

FIGURES

TABLES

Page intentionally left blank

ACRONYMS

CFD	Computational Fluid Dynamics
DLR	Dynamic Line Rating
GLASS	General Line Ampacity State Solver
INL	Idaho National Laboratory
RANS	Reynolds-averaged Navier-Stokes

Page intentionally left blank

Forecasted Dynamic Line Ratings for Regional Transmission Lines

1. Introduction

Transmission line ratings are given by a maximum ampacity based on the maximum conductor temperature limits, which are typically set to avoid sagging or clearance issues of the transmission line segments between structures due to thermal expansion. The dependency of maximum ampacity on the maximum temperature and weather conditions has standard models that were developed by the International Council on Large Electric Systems (CIGRE) (CIGRE 1992; CIGRE 2006; CIGRE 2014), the International Electrochemical Commission (IEC) (IEC 1985) and the Institute of Electrical and Electronics Engineers (IEEE) (IEEE 2012; IEEE 2016).

The weather conditions used in these methods are typically constant values year-round or with seasonal patterns and are set using conservative assumptions for the conditions. By not accounting for additional cooling during periods of high wind or low ambient temperature, there is likely unused head room on many overhead transmission lines. Dynamic Line Rating (DLR) uses a changing line rating based on local conditions rather than a static rating assumption to provide additional ampacity capacity to a transmission line. DLR has been identified by the United States Department of Energy as a distribution infrastructure solution to defer upgrades, support line outages, and increase yields of distributed generation (US DOE, 2010; US DOE 2014).

The conservative nature of transmission line standards and the regional transmission operators (RTOs) can be hard to adjust, so research showing the benefits of DLR is important to prove the benefits of the method. Case studies utilizing weather data in the field has shown potential for DLR to increase ampacity above static throughout several countries (Greenwood et al., 2014; Bhattarai et al., 2017; Bhattarai et al., 2018; Usik-Joustenvuo and Pasonen, 2013; Aznarte and Siebert, 2017) Further studies have involved coupling the weather data with forecast model to be used for forecasted ratings, and assessment of risk (Abboud et al., 2019b).

This study utilizes the coupling of field weather data and weather model data from the High-resolution rapid refresh model (HRRR) within the region of interest with Computational Fluid Dynamics (CFD) results. For the wind field simulations, the steady-state Reynolds-Averaged Navier Stokes (RANS) approach was used for turbulent modelling of the wind flow (Jones and Launder, 1972). The RANS approach has been used to validate wind flows in complex terrains (Wallbank, 2008) with adequate speed up predictions (Dhunny et al., 2016) and low-elevation mountains within acceptable error (Dhunny et al., 2015; Dhunny et al., 2017). Due to the convective cooling calculation, the error in the cooling rate scales as approximate the square root of the wind speed, so a 10% error in wind speed is only a 5% error in the cooling rate.

The weather forecasts used in this study came from version 3 of the HRRR model. HRRR is a convection-allowing forecast model that outputs meteorological variables on a 3-km horizontal grid over the continental United States (Benjamin et al., 2016; Smith et al., 2008). The HRRR was developed at the National Oceanic and Atmospheric Administration (NOAA) Earth System Research Laboratory and is run operationally at the National Center for Environmental Prediction (NCEP). The previous version of the HRRR, Version 3, became operational on 12 July 2018 and outputs forecasts from zero through 18 hours with 15-minute temporal resolution that are updated every hour. The model also outputs forecasts from zero to 36 hours with one-hour temporal resolution at 00, 06, 12, and 18 UTC. While the HRRR version 4 recently became operational and allows for 48-hour forecasts, this was only in December 2020, and will begin to be utilized in the future as more data is available.

In addition to transmission lines for regional power, another benefit to DLR is concurrent cooling effects associated with wind farms. With higher wind speeds, the power generation of wind farms increases while the ampacity of a transmission line is increased due to higher cooling rates. This effect could be used to avoid curtailment of power generation, and some studies have proved this correlation (Cao et al., 2016; Talpur et al., 2015, Banerjee et al., 2015). The previous work detailed the effect specific to the gen-tie lines connecting the wind plants to the regional transmission, and mostly showed this is effect is well correlated due to the proximity of the gen-tie lines to the power transmission (Abboud et al., 2022). This study is focused on examination of the correlation of the concurrent cooling effect specific to regional transmission lines which are much longer in length than the gen-tie lines and it is possible the effects occur at different time periods than the actual power generation. This study will examine three different regional areas in the United States, these are 1) Proposed wind plant near the INL desert site and Snake River Plain 2) Wind plants and transmission corridor in the Columbia River Gorge and 3) Offshore wind plant connection to New York Long Island.

The maps for the regions modeled are shown in Figure 1a for the INL site, Figure 1b for the Columbia River Gorge and Figure 1c for the New York Long Island. The circled north-south line in Figure 1a is the transmission line that the previously modeled gen-tie line connects to for the INL site. For the BPA site, the domain size is large enough four sub domains were created shown in Figure 1b for an original set of 40 transmission lines, but those have been narrowed down to the primary east-west transmission lines in the corridor. The map from NYSERDA shows the offshore wind plant locations, and the proposed interconnection substations, this map was used in conjunction with infrastructure maps of the overhead transmission to determine a pathway for connection for the Empire project, and a longer pathway to connect the Beacon and Sunrise projects, these pathways are shown in Figure 1d, and effectively modeled as a single line for now. In addition to examining the concurrent cooling correlations for the regional transmission lines, the accuracy of the HRRR forecasted ampacity to the observational ampacity will also be assessed.

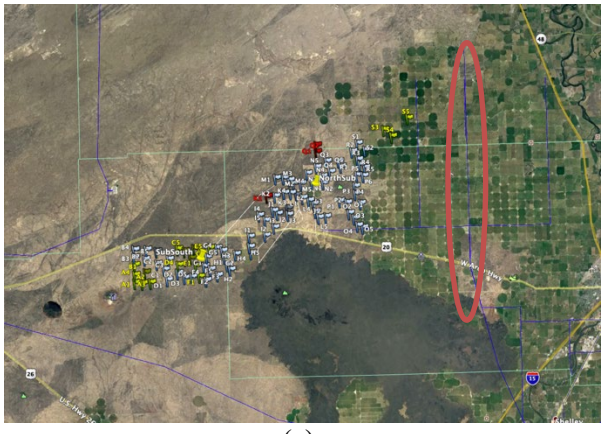

(a)

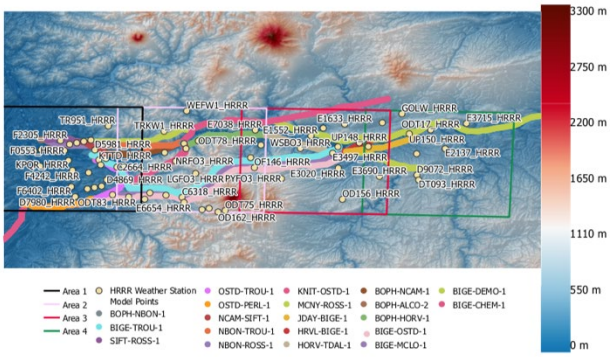

(b)

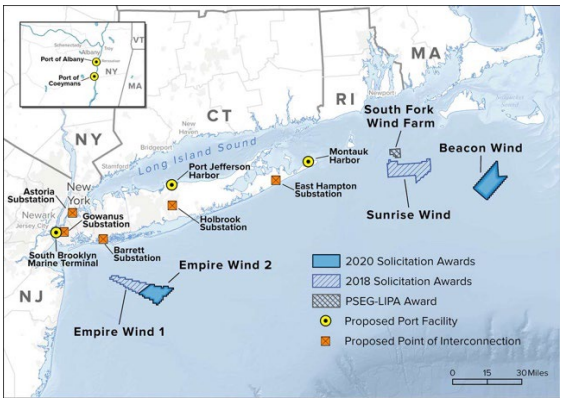

(c)

(d)

Figure 1. The region of interest for the (a) INL site of interest with circled regional transmission line (b) Columbia River Gorge east-west transmission lines and (c) NYSERDA map of the offshore wind projects and substation connections (https://www.nyserda.ny.gov/All-Programs/Offshore-Wind/Focus-Areas/NY-Offshore-Wind-Projects).

2. Study Regions

2.1 INL Desert

The CFD domain for the region is set up as shown in Figure 2. The transmission line of interest runs north-south between two substations. Figure 2a shows the elevation map with the nearby weather station locations as circles and transmission line midpoints as squares, Figure 2b shows the corresponding HRRR model point locations, and Figure 2c shows the roughness layer, which consists of the city and surrounding farmland. The domain size used is a 60 km by 60 km box. The elevation map scale is in meters showing low areas and green, and high areas, such as nearby buttes in brown. The roughness layer shows regions of low to high vegetation and cities where near ground wind fields would be affected. These regions are not explicitly modelled in the CFD, so the roughness layer is used to approximate slowdowns due to these subgrid effects. This value is set to 1.0 for city regions (dark red on the scale), 0.8 for heavily forested areas (red on the scale), 0.1 - 0.2 for farmland or plains covered in shrubs (yellow on the scale) and set to 0 (white on the scale) for flat areas, such as along the water surface, and for areas with very little vegetation. The roughness values are used in the log- law correlations for the boundary layer with values adapted from Troen and Petersen, 1989. A proposed wind plant sized at 450 MW was previously modeled (Abboud et. al, 2022) and that data will be used to assess the concurrent cooling effect on this line.

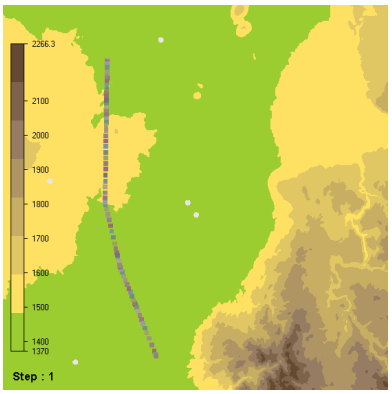

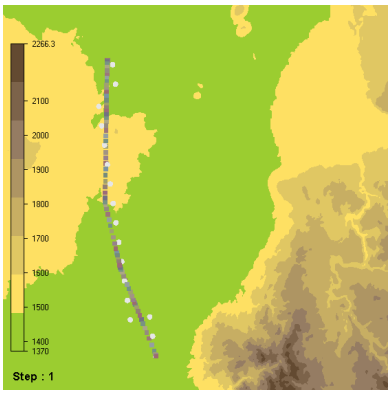

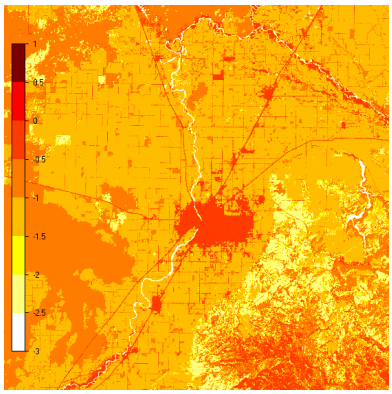

(a) (b) (c)

Figure 2. The region of interest modeled for the transmission with (a) terrain elevation and weather station locations, (b) terrain elevation and HRRR model locations, and (c) roughness layer.

The maximum conductor temperature for the rating is 100 C, with an emissivity and absorptivity both equal to 0.5, it is assumed to use a Drake ACSR conductor. For the static rating, the constant weather parameters assumed a wind speed of 2 ft/sec perpendicular to the conductor, 25 C ambient temperature, and 96 W/ft^2 solar irradiation.

2.2 Columbia River Gorge

The Columbia River Gorge site of interest for the wind power production is a 60km x 60km subset that contains 15 wind farms. These wind farms are each given a conductor that is sized according to basic static ratings to have a capacity large enough to maintain the specified power production. The power generated was estimated using high-resolution rapid refresh (HRRR) forecasting models and historical weather data from the MesoWest tool. For the total region of transmission lines to reach from the wind plants to the Portland/Vancouver metro area the total domain size is over 200 km in east-west direction. This requires uses a decomposition to run through WindSim, the terrain elevation for the four subdomains is shown in Figure 3a-d, and the roughness layer for these sub domains is shown in Figure 3e-h. The maximum height varies substantially from 1316, 3345, 2132, to 945 m above sea level from west to east. The elevation maps also show the HRRR model points along the transmission lines of interest, and some selected transmission lines. The roughness layer shows a wide gradient moving from urban areas in the west to forested areas in the center out to rural farmland on the eastern edge of the domain.

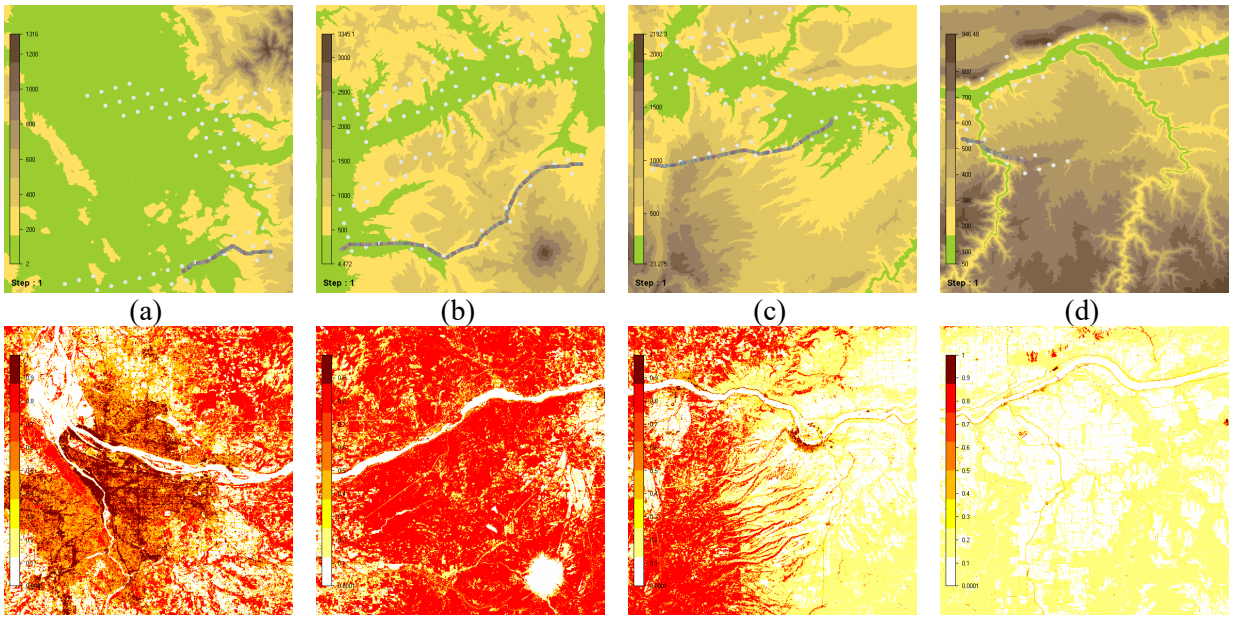

(a) (b) (c) (d)

(e) (f) (g) (h)

Figure 3. The region of interest modeled for the Columbia River Gorge showing the (a-d) elevation of the terrain from west to east, and the (e-h) roughness layer of the terrain from west to east.

The wind farms for the region have been previously modeled in in Abboud et. al, 2022, and that power generation data is used here.

2.3 New York Long Island Offshore Wind

Through surveying proposed offshore wind projects on the eastern coast, the projects to be constructed off the coast of New York's Long Island appear to be a good case study for considering as a DLR application. This is because of the large size of these projects, as well as New York state's goal of continuing to expand its offshore wind power. Through a legislative mandate, by 2035 the state will increase its offshore wind capacity to at least 9,000 MW, the largest of any state. Since most of the power needs are within the New York City itself, and the offshore wind plants are off the coast of Long Island, this requires an examination of a long corridor of overhead transmission lines across the island into the city itself.

The initial assessment will include the four largest solicitation awards by NYSERDA. These are the Empire Wind 1 and Empire Wind 2 project that provides 816 MW and 1260 MW capacity off the southern coast of the island to the Gowanus substation in Brooklyn, as the well as the Sunrise Wind project that provides 880 MW capacity off the island's eastern coast and connects to the central Holbrook substation, and the Beacon Wind project that will supply 1230 MW of capacity connected to the Astoria substation in Queens.

As with prior sites that have been studied by INL, the Homeland Infrastructure Foundation Level Data (HIFLD) can be used to determine the primary transmission lines of interest that can be modeled with DLR. The Empire Wind connections can be modeled by running an overhead line along existing corridors from the Barret substation to the Jamaica substation, since the connection from Jamaica to Gowanus is an underground transmission line. For the Beacon Wind project, this same endpoint can be used as the Jamaica to Astoria connection is also through underground transmission. The Sunrise wind is connected to the Holbrook substation and the corridors here are all overhead transmission lines. The map for the transmission line layout for Long Island is shown in Fig. 4.

Figure 4. Map of the transmission lines across New York's Long Island.

The extent of the full CFD model has been determined to build out the terrain and roughness layers within the CFD code. Fig. 5a shows the full-scale terrain that is wide enough to encompass offshore wind locations in addition to the Long Island transmission corridor. Figure 5b also shows the roughness layer for the region for the near-ground corrections in the CFD model.

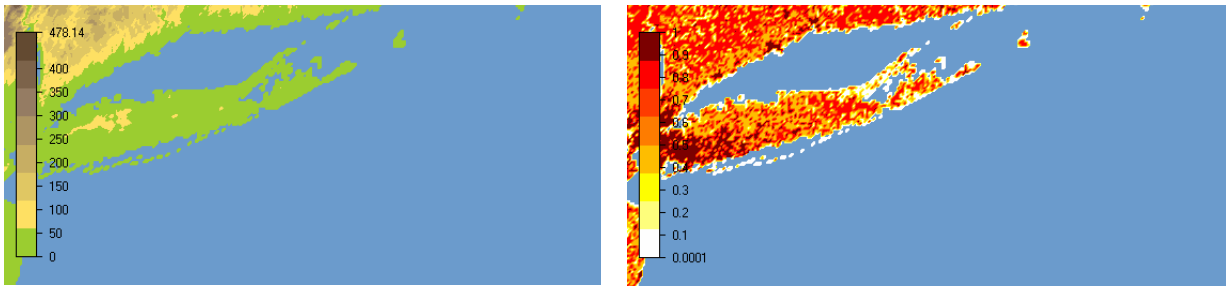

(a) (b)

Figure 5. Terrain map used for the wide region to encompass offshore wind farms and roughness layer.

As with other studies the total domain is decomposed into smaller regions such that each portion can be ran with the CFD code separately to achieve better near ground resolution that what could be accomplished with the full regional model. It was determined that utilizing 50 km x 50 km boxes with a horizontal spatial resolution of 50 m should be sufficient to create four domain boxes around Long Island for the modeling efforts. These domains contain small offsets in the north-south direction of the domain. This region has only minor elevation changes, with the maximum only 164 meters above sea level. Creating a more resolved domain would cut off enough of the shoreline that the model would have to be built with 8-10 CFD domains. The domains to be modeled for the approach are shown in Fig. 6a-d for elevation and Fig. 6f-g for the roughness layer. The process of extracting needed weather data for calculating DLR ratings was done with MesoWest data set that has been used in previously modeled regions. This contains 72 weather stations with publicly available data near the transmission lines to be modeled.

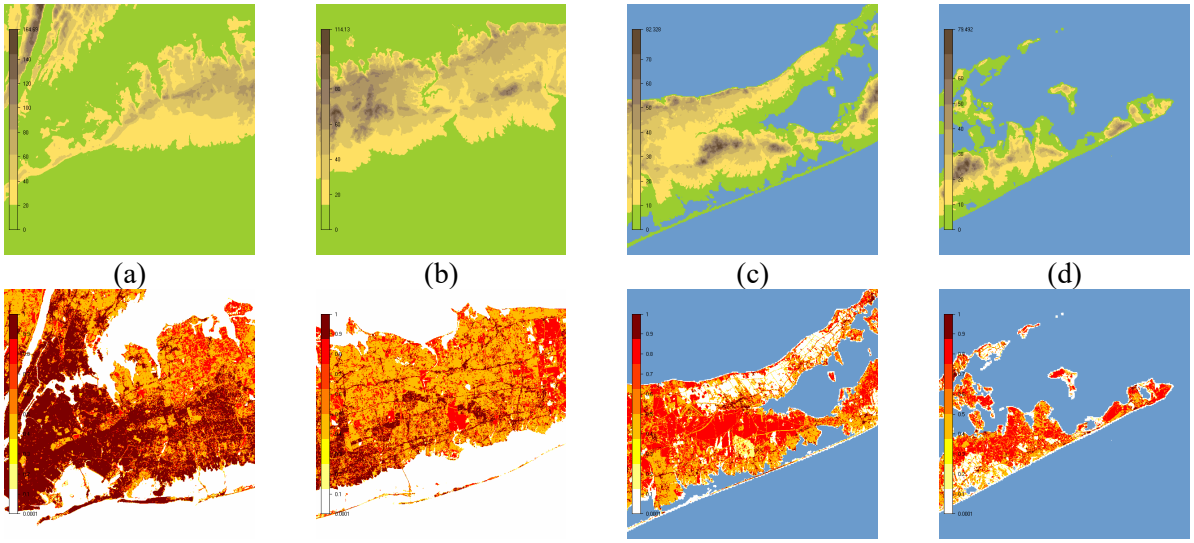

(a) (b) (c) (d)

(e) (f) (g) (h)

Figure 6. Doman decomposition of Long Island into 4 sub domains for the (a-d) terrain and the (e-h) roughness layers. Maximum elevation from left to right is 164, 114, 82, and 79 meters.

3. Methodology

3.1 Line Rating

The equations for DLR are the same used for static rating, based on a simple heat balance for a transmission line. For the weather data, the output is at 5-minute intervals. For the HRRR model data the data output is only done in hourly intervals. The heat balance equation is used to solve for the maximum current, *I*, to get (IEEE, 2012)

$$I = \sqrt{\frac{q_c + q_r - q_s}{R(T_c)}} \tag{1}$$

Where q_c, q_r, and q_s are the convective, radiative and solar contributions, and *R* is the conductor resistance as a function of the conductor temperature T_c. The radiated heat loss per unit length in units of W/m is given by

$$q_r = 17.8D\epsilon\left[\left(\frac{T_c + 273.15}{100}\right)^4 - \left(\frac{T_a + 273.15}{100}\right)^4\right] \tag{2}$$

Where ϵ is the emissivity, T_a is the ambient air temperature and D is the conductor diameter. The heat gain through solar irradiance is given by

$$q_s = \alpha Q_{se} \sin(\theta) A' \tag{3}$$

Where α is the solar absorptivity, Q_{se} is the total solar and sky radiated heat flux corrected by elevation, θ is the effective angle of incidence of the sun's rays and A' is the projected area of the conductor. The convective heat loss is calculated using one of three equations for high wind speeds, low wind speed (below 3 mph) or natural convective cooling. For high wind speed the equation is given by

$$q_{c1} = \left[1.01 + 1.35\left(\frac{DV_w\rho_f}{\mu_f}\right)^{0.52}\right] k_f K_{angle}(T_c - T_a) \tag{4}$$

For low wind speed the equation is given by

$$q_{c2} = 0.754\left(\frac{DV_w\rho_f}{\mu_f}\right)^{0.6} k_f K_{angle}(T_c - T_a) \tag{5}$$

Or for natural convection the equation is given by

$$q_{cn} = 3.645\rho_f^{0.5} D^{0.75}(T_c - T_a)^{1.25} \tag{6}$$

Where V_w is the speed of air, with fluid parameters density ρ_f, viscosity μ_f and thermal conductivity k_f calculated at the ambient temperature. And K_{angle} is the wind direction factor which can vary from about 0.3 to 1.0 based on parallel or perpendicular wind flow to the transmission line, given by

$$K_{angle} = 1.194 - \cos(\phi) + 0.194\cos(2\phi) + 0.368\sin(2\phi) \tag{7}$$

Where ϕ is the angle of incidence between the wind and the transmission line midpoint. The GLASS code developed by INL does all of these calculations for every single transmission line midpoint of interest. The minimum value among all the midpoint calculations is assumed to be the ampacity for each line. To assess the concurrent cooling for regional lines without a static load, the wind power generation is normalized to zero to 1 based on 0-90% of capacity, and the dynamic line rating is normalized to 1 based on the minimum value up to 20% above the static rating. The subtraction of these two normalized variables then shows the correlation between excess DLR capacity and maximum power output, with any value above zero showing the DLR capacity is higher enough to handle 20% over static when the wind plants are operating a peak efficiency.

3.2 Computational Fluid Dynamics

The CFD domain for all the sites modeled uses a vertical resolution that is spaced such that near the ground the resolution is in 5-meter increments to allow for accurate wind fields near the transmission lines, while above 100 meters a log scale is used up to the atmospheric boundary layer. The domain sizes for the CFD model are

- INL Site: single domain 60 km by 60 km at 60 m horizontal resolution
- CRG: 210 km by 60 km split into 4 domains at 50 m horizontal resolution
- NYLI: 185 km by 85 km split into 4 domains at 50 m horizontal resolution

The steady-state standard *k*-ε RANS model is used for modelling the turbulent kinetic energy and dissipation rate. The PDEs for the solution consist of the velocity vectors, the continuity equation, and equations for the turbulent kinetic energy and turbulent dissipation rates. The equation for the velocity vectors is

$$\rho U_i \frac{\partial U_j}{\partial x_i} = \frac{\partial}{\partial x_i}\left[(\mu + \mu_t)\left(\frac{\partial U_i}{\partial x_j} + \frac{\partial U_j}{\partial x_i}\right)\right] - \frac{\partial p}{\partial x_i} \tag{9}$$

The turbulent kinetic energy, k, equation is given by

$$\frac{\partial (U_i k)}{\partial x_i} = \frac{\partial}{\partial x_i}\left[\frac{\mu_t \partial k}{\sigma_k \partial x_i}\right] + P_k - \epsilon \tag{10}$$

And the equation for the turbulent dissipate rate, ϵ, is given by

$$\frac{\partial (U_i \epsilon)}{\partial x_i} = \frac{\partial}{\partial x_i}\left[\frac{\mu_t \partial \epsilon}{\sigma_\epsilon \partial x_i}\right] + c_{\epsilon 1}\frac{\epsilon}{k}P_k - c_{\epsilon 2}\frac{\epsilon^2}{k}P_k \tag{11}$$

Where the turbulent viscosity is given by

$$\mu_t = \frac{C_\mu k^2}{\epsilon} \tag{12}$$

And the turbulent production term is given by

$$P_k = \mu_t \left(\frac{\partial U_i}{\partial x_j} + \frac{\partial U_j}{\partial x_i} \right) \frac{\partial U_i}{\partial x_j} \tag{13}$$

Where c_μ, c_{ϵ_1}, c_{ϵ_2}, σ_k, and σ_ϵ are the fixed constants for the model, with values set to 0.09, 1.55, 2.0, 1.0, and 1.3, respectively (Jones and Launder, 1972).

4. Results

4.1 INL Site

The wind data for two of the weather stations that are in the central regional of the line and therefore used for most of the midpoint DLR calculations are shown in Figure 7. Figure 7a shows the Kettle Butte site which is approximately halfway between the wind farm and the regional transmission line, and Figure 7b shows the corresponding HRRR location. The wind data here is in good agreement with the prevailing wind direction, and while the HRRR data is under predicting measured wind speeds, it should be noted the site is at 15-meter elevation rather than the 10 meters that HRRR output provides. Figure 7c shows the tower at the Idaho Falls airport, which shows a similar trend with prevailing wind direction captured well, but with slightly lower wind speeds, again due to the 15-meter versus 10-meter heights.

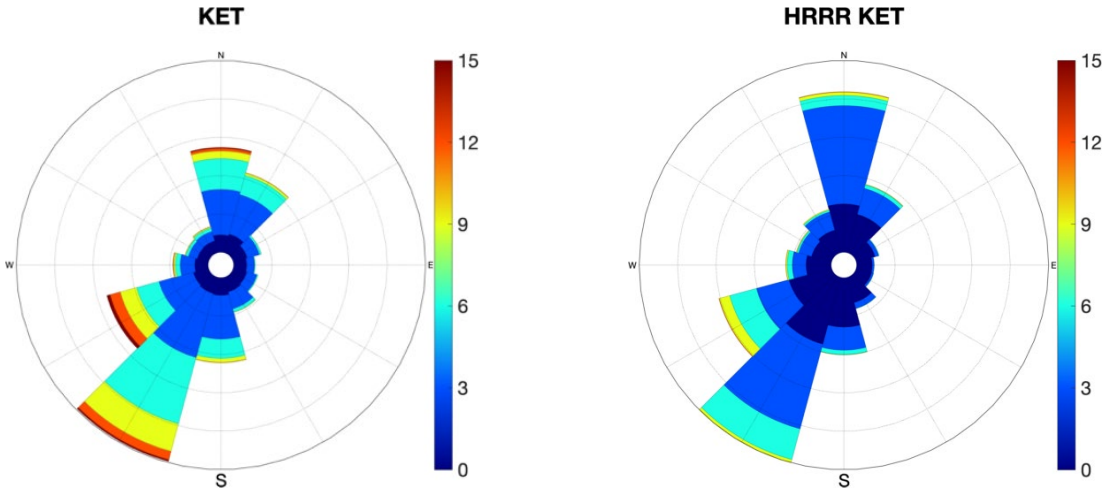

(a) (b)

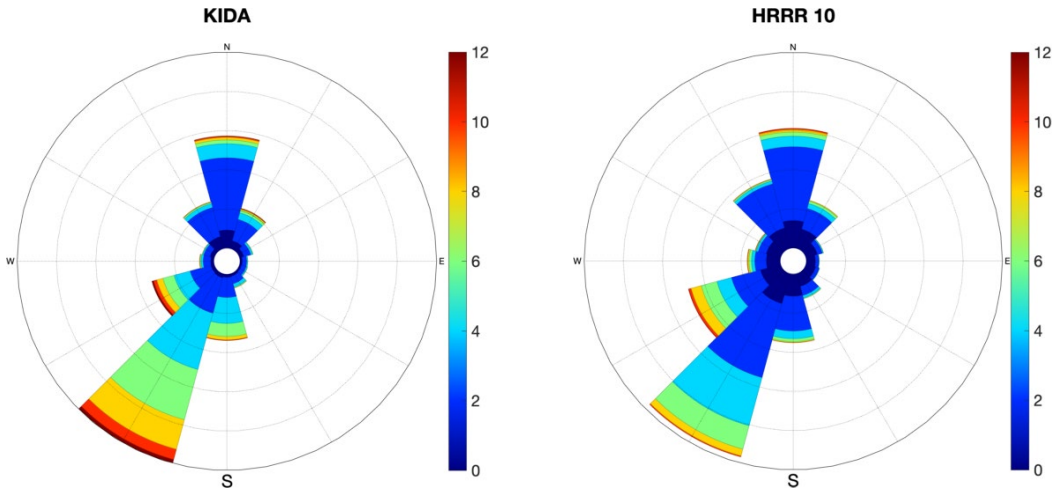

(c) (d)

Figure 7. The Kettle Butte (a) weather station data wind statistics compared to the (b) closest HRRR data point, and the (c) IDA airport weather station data wind statistics compared to the (d) closest HRRR data point.

The results for the CFD wind fields are shown in Figure 8 for the domain of interest on the INL site. The data shown is for the north, east, south and west incoming wind vectors. There are eight additional sectors models at 30-degree spacing, but these are left out for brevity. The wind data is shown for the 10-meter height for the regional transmission lines. CFD data for the turbine heights is included in Abboud et. al, 2022. The southern end of the line shows some speed up and slow down effects from the hills to the southeast, but other than that the wind speed from the CFD results shows very minor changes over the region where the transmission line is located.

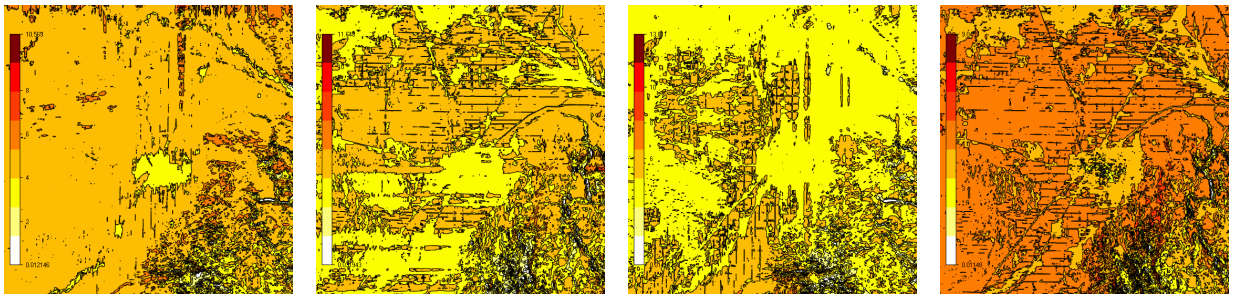

(a) (b) (c) (d)

Figure 8. The CFD wind data for the INL site region for incoming (a) north, (b) east, (c) south and (d) west wind direction.

The raw ampacity data for the regional transmission line is calculated over a 3-year period for the weather observational data. The HRRR forecast that is 3-hours in advance is the shortest timeframe for which the forecasted data can be simulated and made available on the NOAA database for use is representative of a near term forecast and labeled as the HRRR3 dataset. The HRRR forecast that is taken at noon on day 0 for a 36-hour hour period provides the day-ahead forecast from hours 12-36 corresponding to midnight-to-midnight on the next day, this is effectively the day-ahead forecast from the HRRR model and labeled as the HRRR36 data set. Figure 9a shows the raw ampacity for the

observational data, Figure 9b shows the raw ampacity for the HRRR3 data and Figure 9c shows the ampacity for the HRRR36 data. Since the HRRR36 came online more recently only 1.25 years of data are plotted. The dotted black line in the plots shows the static rating for the line. The DLR rating remains well above static across fall, winter and spring months, and only dips below for periods in the summer.

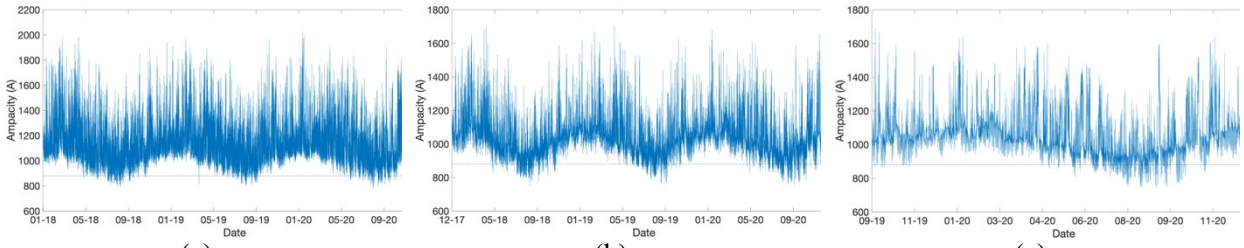

Figure 9. The raw DLR ampacity data for the (a) weather observation data the (b) HRRR3 forecast data, and the (c) HRRR36 forecast data.

The raw data from the ampacity is then processed and tabulated to determine the fraction of time that the DLR ampacity remains above static. This data is shown for all three sets of data in Figure 10. The observational data shows a DLR rating above static for roughly 98% of the time, with an average rating 249 A over the static. The two forecast data sets show a slightly lower ampacity than the observed and are in good agreement with each other. The forecasted data still shows significant headroom over static rating about 94% of the time, with an average ampacity 163 A over static for the HRRR3 and 171 A over static for the HRRR36 forecasts.

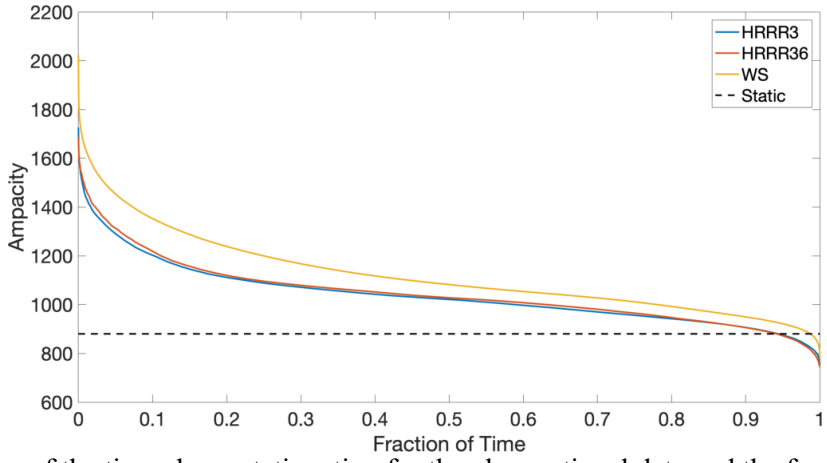

Figure 10. Tabulation of the time above static rating for the observational data and the forecasted data.

The HRRR datasets are interpolated to the same timeframe as the observational datasets with a 15-minute moving average applied. The forecasted data is then subtracted from the observed data to determine the error. The raw error for the forecast data is shown in Figure 11a for the HRRR3 dataset and in Figure 11b for the HRRR36 dataset. The error is mostly contained in a small oscillating region of 100-200 A, but has many large outlying data points that can occur when the forecasted and observed wind speed differs significantly. The mean absolute error was calculated to be 106 A, or 9.4%, for the HRRR3 forecast and 110 A, or 9.7% for the HRRR36 forecast.

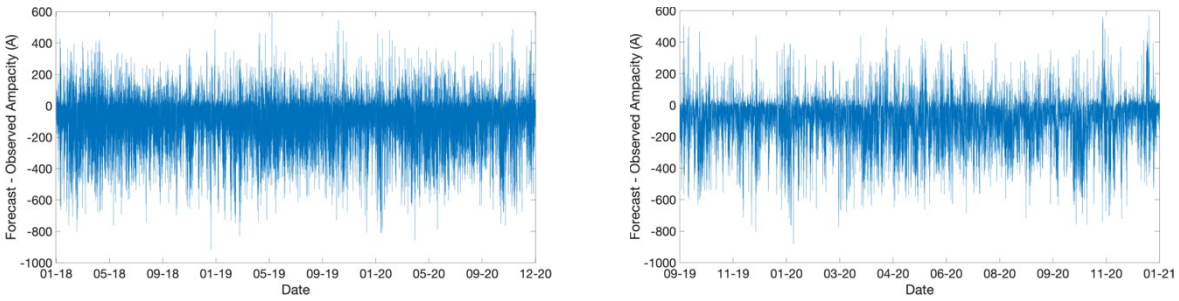

Figure 11. The raw forecasting error for (a) HRRR3 forecast and the (b) HRRR36 forecast.

The previously modeled wind power data was then plotted against the ampacity data to determine the effects of concurrent cooling for the regional line. Figure 12 shows both the power generation and the observed DLR ampacity. Without the load data for the line, it's hard to determine the exact benefit of the concurrent cooling. To get around this, the wind power generation data and the ampacity data were both normalized as described in Section 3. It is assumed than any extra cooling on the transmission line above 20% of static would require no additional curtailment of the system. With the normalized variable anytime it dips below 1, then the rating is less than 120% of the static. The normalized variables are plotted in Figure 13a for the full time period, from which is becomes hard to discern the effect. The normalized variables are plotted in small time frame segments in Figures 13b-d for spring, summer and winter months. For the winter months, the normalized DLR rating never dips below the normalized wind power generation, which means that 120% of the static rating is always available in the wind generation is peaked. For the spring and summer months there are times where the variable goes under one where curtailment might be needed, however, when compared to the normalized power generation, these dips often occur when the wind power generation is minimal. Though there a few instances where the DLR dip occurs when wind power generation is peaked which might lead to curtailment depending on the total load.

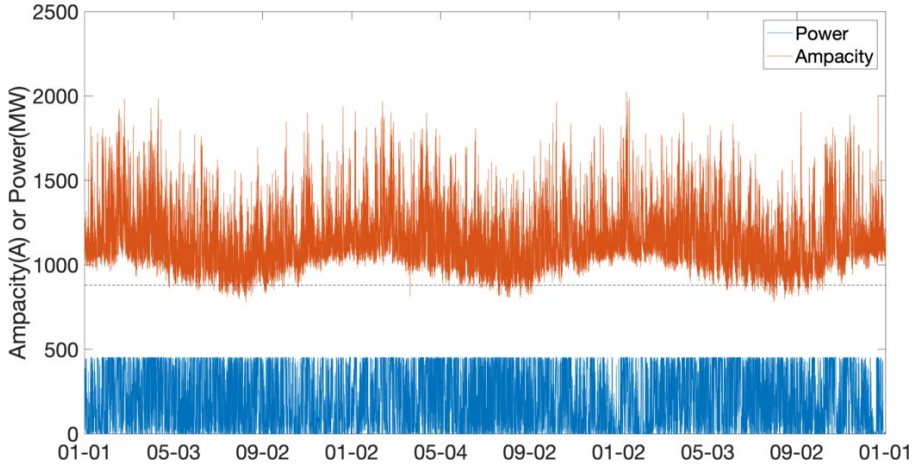

Figure 12. The wind power generation shown in blue, and the observed ampacity shown in red.

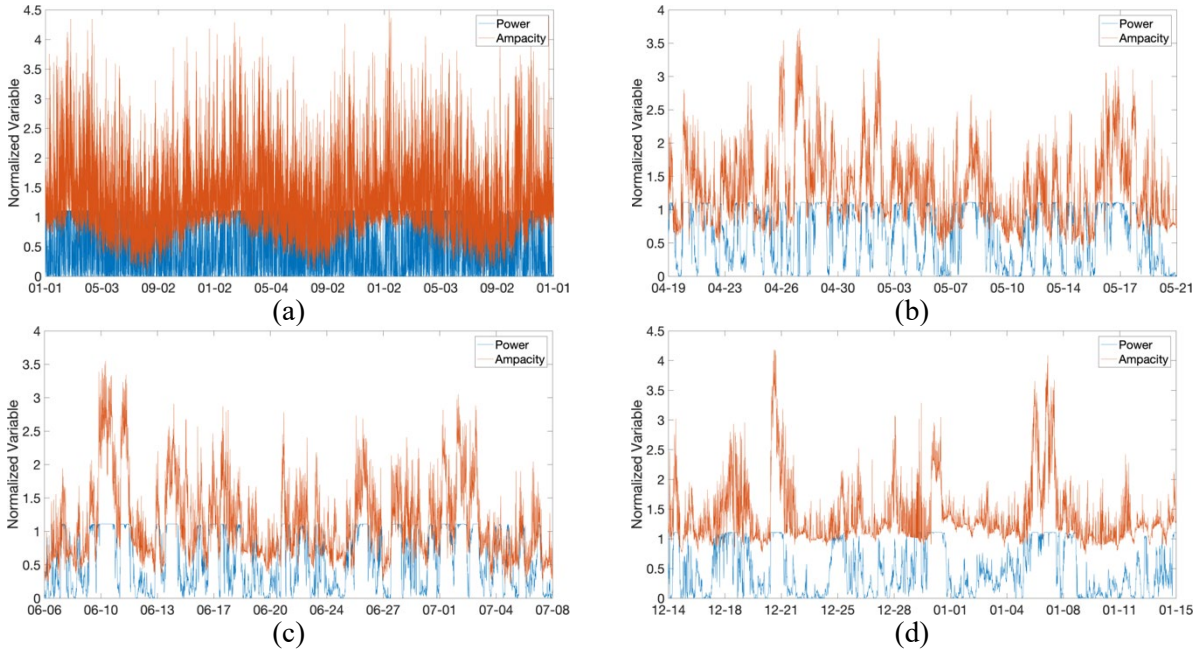

Figure 13. The normalize wind power generation and ampacity for the (a) full period, (b) selected spring months, (c) selected summer months, and (d) selected winter months.

As with the raw data this tabulated can also be tabulated to be turned into a histogram to determine the total amount of time that the DLR is above static when the wind power generation is peaked, which points to beneficial effects of concurrent cooling allowing for additional load without curtailment or additional capital expense such as re-conductoring a line. The data for the subtraction at a normalized 120% of static is shown in Figure 14a, with the cumulative density function (CDF) shown in Figure 14b. The value of the CDF is 0.07 at a value of zero, this is the fraction of time that the normalized DLR variable is less than the normalized wind power generation, and potential curtailment could be needed. The normalized variable is also tested with a 110% of static value, and shown in Figure 14c, with Figure 14d showing the CDF. If only 10% above static is needed on the regional line for this load, the fraction of time that curtailment would be needed then drops drop to 0.014.

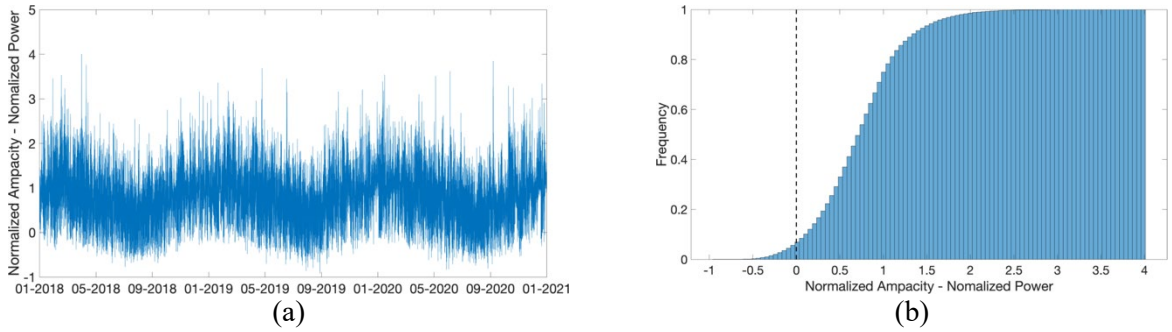

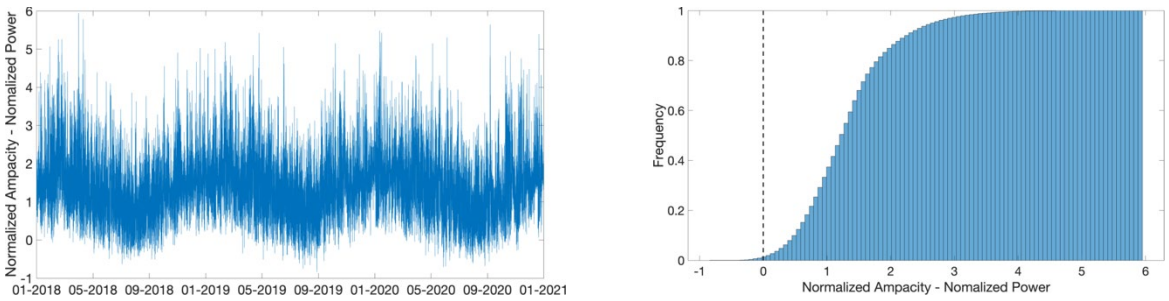

(c) (d)

Figure 14. The (a) raw normalized 120% static ampacity minus normalized power generation, (b) CDF showing amount of time greater than 0, (c) raw normalized 110% static ampacity minus normalized power generation, and (d) CDF showing amount of time greater than 0.

4.2 Columbia River Gorge

The weather data and the forecast data for regions the weather stations that were nearby the turbines of interest were directly compared to give an error in the predicted ampacity calculation between utilizing forecast and observational weather data for the region. The uncertainty for the weather stations in the Columbia River Gorge region that are nearby the wind farms are shown in Table 1.

Table 1. Uncertainty of Columbia River Gorge ampacity forecasts.

Station	3-hour uncertainty	36-hour uncertainty
E0859	16.5%	21.3%
E2137	15.3%	17.6%
D9072	5.7%	6.8%

After performing quality assurance tests on the weather stations that are within the BPA region of interest, serval weather stations in the area had to be ignored due to large gaps in the available data, long periods (i.e., months) of bad or zero speed wind speed data or other issue. Upon completing the analysis, all but three weather station sites within the domain of interest were thrown out. In this region of Oregon/Washington, the population density is extremely low, so no high-quality observations such as those typically available from the National Weather service, or local state governments such as the department of transportation were available. All three weather stations were from the citizen network, that does not have rigorous standards. The wind roses for these weather stations are shown in Figure 15. Figure 15 also shows the corresponding wind roses for the closest HRRR model data points to these weather station locations. E0859 and E2137 are near the north end of the site along the river and the direction is mostly west-to-east, this is mostly in agreement with the HRRR models, though are shifted by about 30 degrees. The D9072 is on the south end of the site further from the river gorge and shows a wider spread in directions. For this site, the HRRR model does overpredict the wind speed more than the other two. An overall comparison between the INL site and the Columbia River Gorge region shows significantly lower wind speeds in this region.

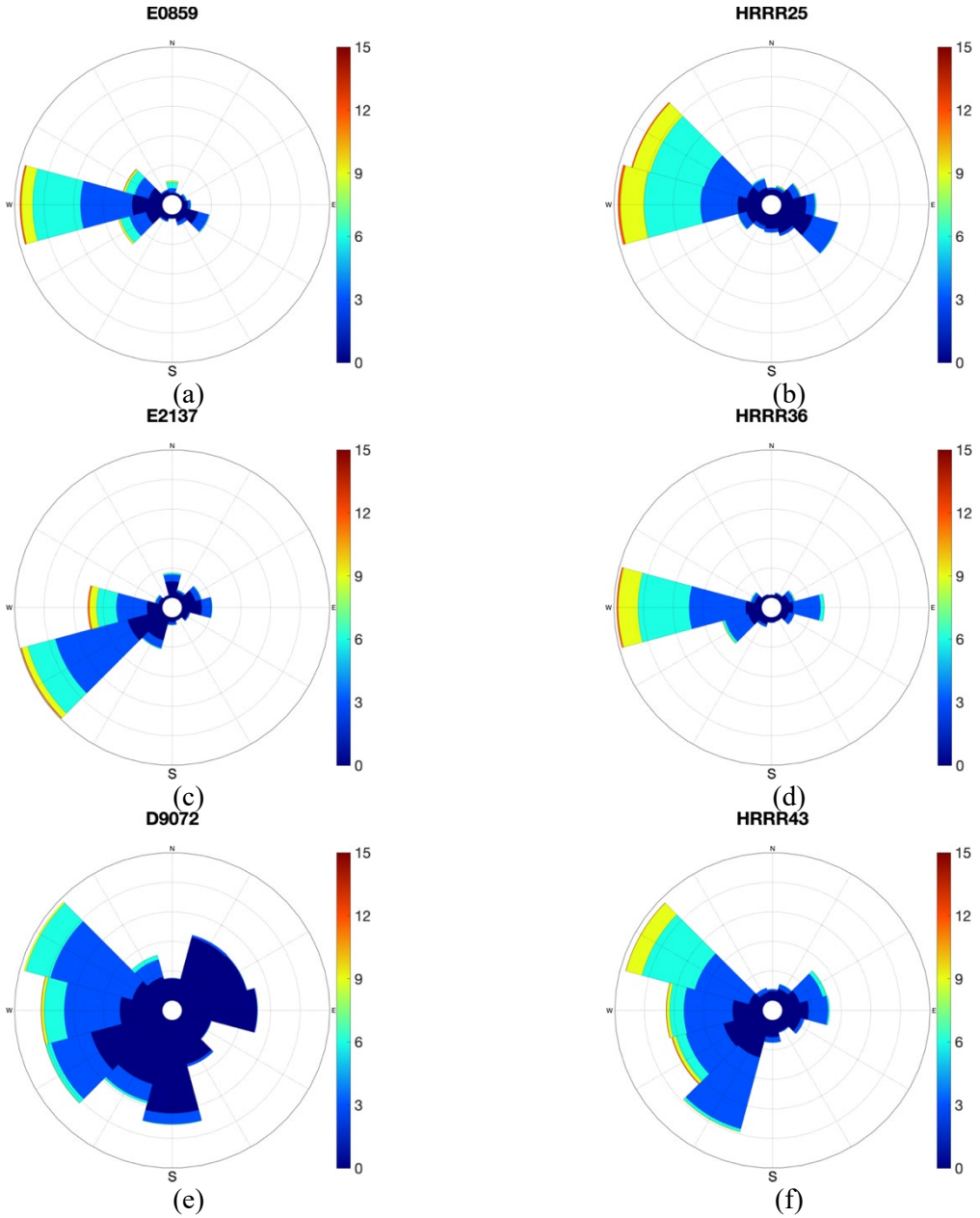

Figure 15. The wind roses for the weather stations in the Columbia River Gorge (a) E0859 and (b) HRRR model point near E0859, (c) E2137 and (d) HRRR model point near E2137, (e) D9072 and (f) HRRR model point near D9072.

The results for the CFD wind fields are shown in Figure 16 for the site along the Columbia River. The data shown is for the north, east, south and west incoming wind vectors. There are eight additional sectors models at 30-degree spacing, but these are left out for brevity. The wind data is shown at two different heights, 10-meters above ground level – corresponding to the height of the transmission lines, and at 100-meters above ground level. The wind plants modeled in the BPA region vary in hub height from 65-100 meters, and those corrections are included within the WindSim CFD model. The variability in the wind speed across the BPA region is much higher than that of the INL site, which is mostly flat, with the exception of the buttes. As seen in the lower set of images up at 100m, this variability remains consistent.

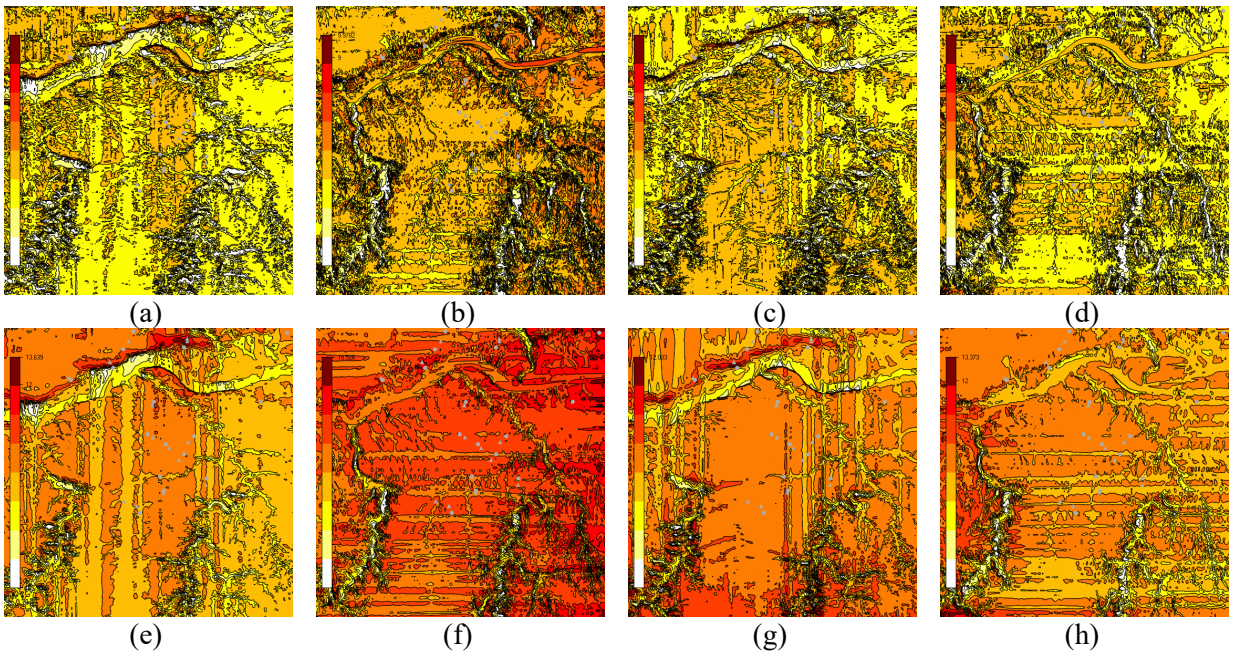

Figure 16. The CFD results for the heights corresponding to the gen tie lines for incoming (a) north, (b) east, (c) south and (d) west incoming wind, and the CFD results for the heights corresponding to the wind turbines for incoming (e) north, (f) east, (g) south and (h) west incoming wind for the BPA region.

While BPA does not have the individual transmission-line loads available online to assess the curtailment possibilities directly, the entity does have total loads divided into power flow gates as shown on the map above. The image shows the wind flow gate data from BPA plotted against the total wind generation of the modeled wind farms over a weeklong period, and the lose correlation of the wind farm data and the power loads shows that the mapping from BPA's flow gates to our modeled wind farms appears correct and will provide a basis for dividing out data to individual line segments. Thew power flow gate data also has various regions along the Columbia Gorge as shown in the second image, these power flow gates increase in total load moving from east to west along the gorge. This type of data may be used to narrow down specific segments of interest for curtailment. This is shown in Figure 17 and Figure 18.

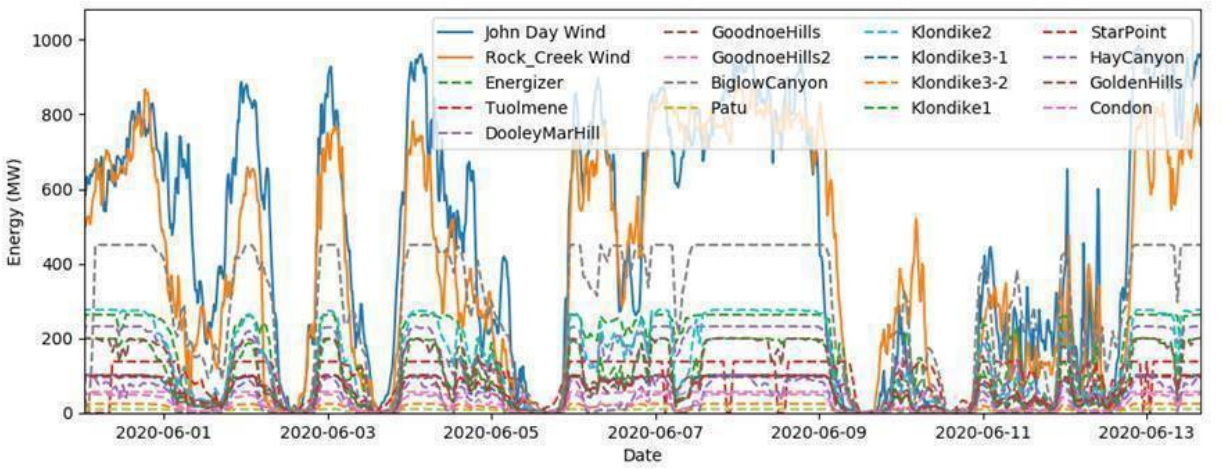

Figure 17. Comparisons of wind farms modeled to nearby flow gate information.

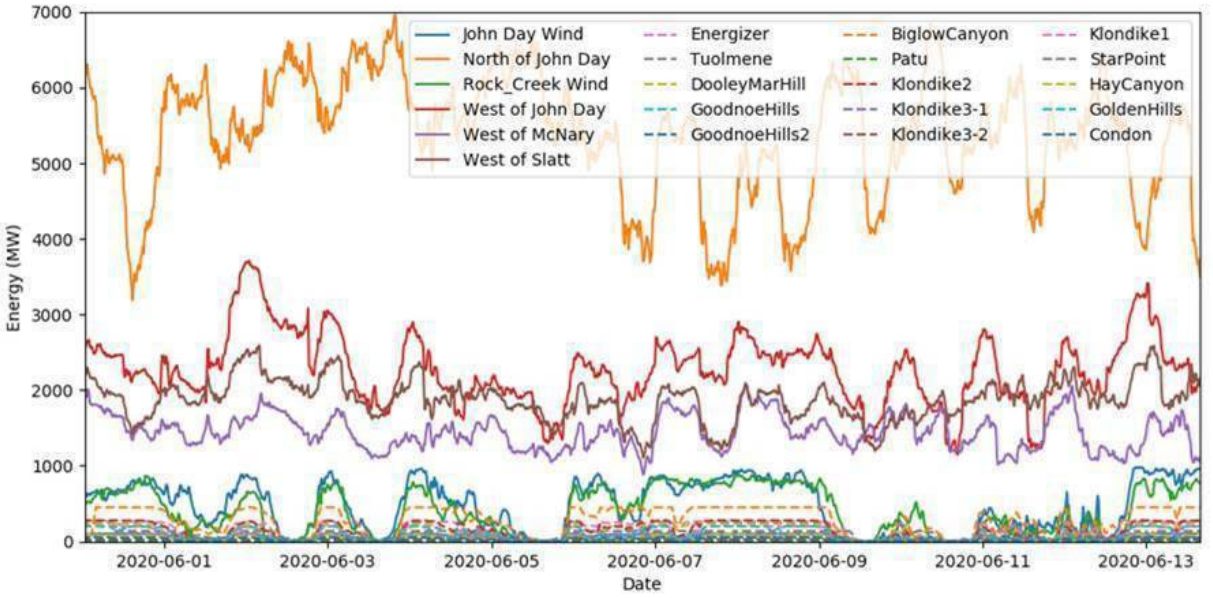

Figure 17. Comparisons of wind farms modeled to all flow gate information.

The original set of transmission line was narrowed down to only the set that geographically passes through the Slatt and John Day flow gates, as these are the closest to the wind farms that were modeled. Over a 1-week period, the plot shows the comparison of the total DLR calculated ampacity along these flow gates overlaid on the total wind power generation of the wind farms modeled with the HRRR forecast data. While some of these modeled regional transmission lines stretch 10s of kilometers across the terrain, high wind speed is still present across these lines far away from the wind farms. This leads to a very high correlation of the modeled wind farm power generation and the calculated DLR ratings for the regional transmission lines. Separating out the total loads and voltage of the individual lines will allow for further analysis of the capacity in the future. This is shown in Figure 18.

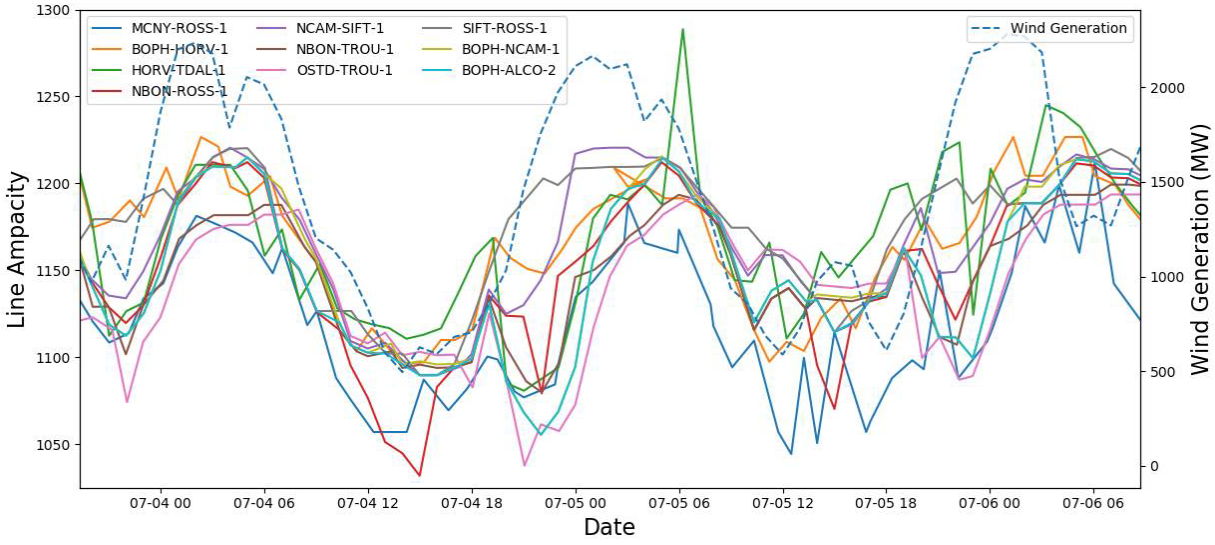

Figure 18. DLR line ampacity through the flow gate compared to toral power of wind farms modeled. Solid lines show transmission line ampacity and dashed lines show wind power generation.

While BPA does not have the individual transmission-line loads available online to assess the curtailment possibilities directly, the entity does have total loads divided into power flow gates. The correlation between the HRRR-36 modeled wind farm power generation and the BPA flow gate data is shown over a 10-day period in Figure 19. The correlation of the wind farm data and the power loads shows that the mapping from BPA's flow gates to our modeled wind farms appears correct and will provide a basis for dividing out data to individual line segments. The power flow gate data also has various regions along the Columbia Gorge, these power flow gates increase in total load moving from east to west along the gorge. This type of data may be used to narrow down specific segments of interest for curtailment. The raw ampacity for the major lines is shown in Figure 20a, and the tabulated time for the rating is shown in Figure 20b.

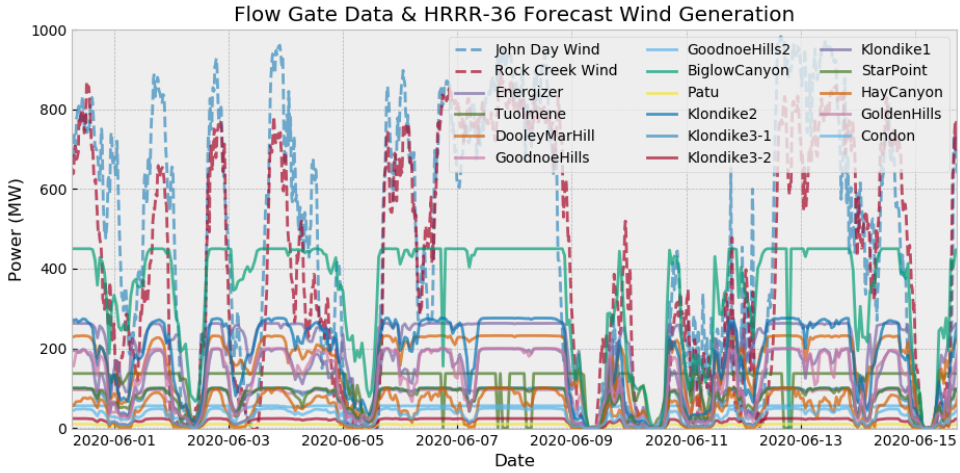

Figure 19. Comparisons of flow gate data (dashed lines) and HRRR-36 wind power generation (solid lines).

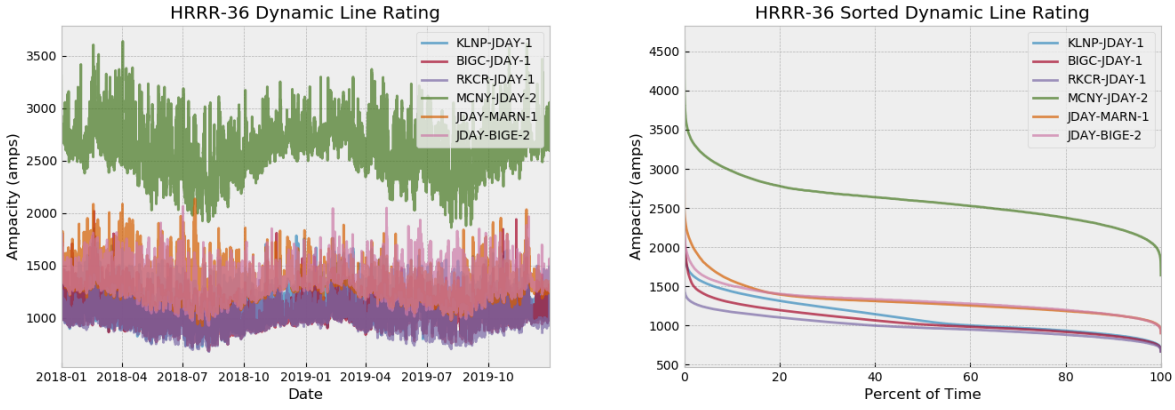

(a) (b)

Figure 20. The (a) timeseries HRRR-36 hour forecast DLR and the (b) accumulated ampacity as a function of time.

In the area covered in this study there are 4 flow gates of power flow data considered: John Day Wind, Rock Creek Wind, West of John Day, and West of McNary. The timeseries flow gate data over a three-year period is shown in Figure 21. Here, it can be seen that the wind flow gates follow different characteristics than the other two flow gates. In general, they fluctuate between zero and a maximum power flow that is the size of wind generation they are connected to (Fig. 3). On the other hand, West of John Day and West of McNary are more likely influenced by the bulk power demand and hydro generation in the area.

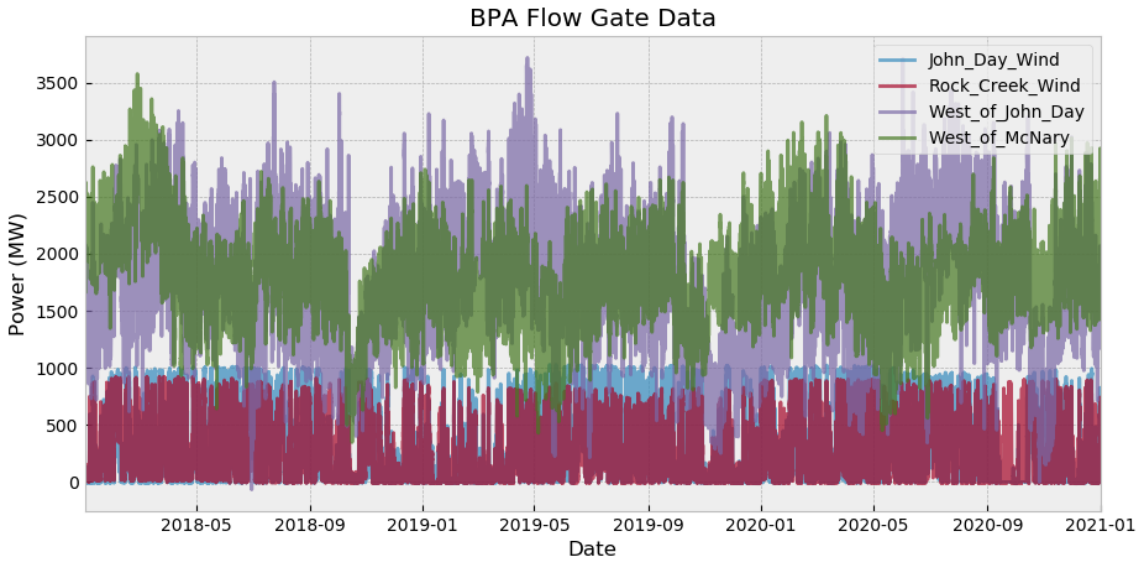

Figure 21. Timeseries BPA flow gate data over a three-year period.

The high correlation of the wind flow gates and the wind generation is also strongly coupled with the DLR of the transmission lines as seen in Figure 22a. Here, the John Day Wind flow gate data and the DLR of the two transmission lines over a two-week period is shown. Figure 22b shows the West of Jon Day flow gate, here there is a lower correlation between the flow gate and DLR in the West of John Day lines. It is likely that these lines are responsible for the bulk of the hydro generation in the area but are affected by the wind generation as well.

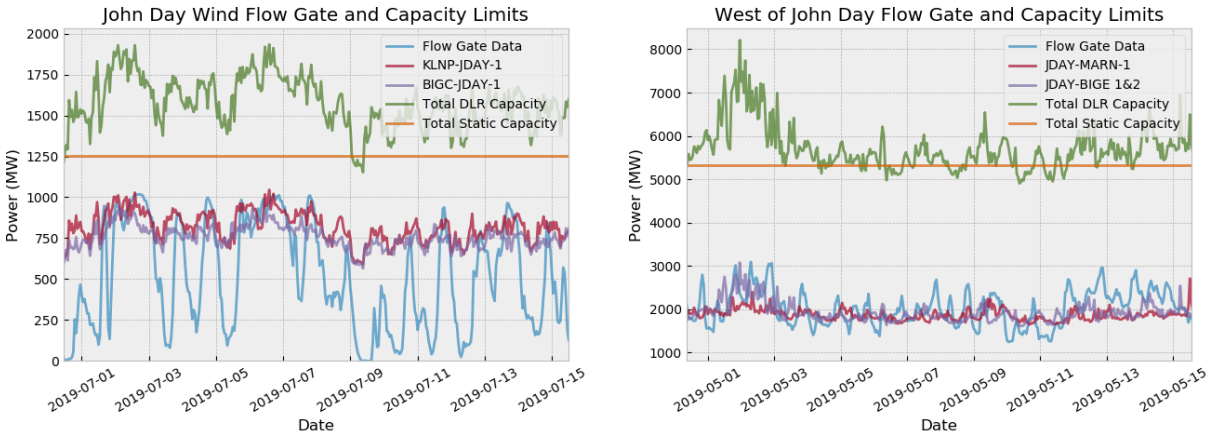

Figure 22. The (a) high correlation between John Day Wind flow gate and DLR and (b) lower correlation of West of John Day flow gate and DLR.

The amount of additional power flow available for DLR in relation to static ratings for each of the flow gate lines is shown in Table 1. Here, the hourly DLR capacity is the average over the two-year period. The result indicates that there is a 9 to 22% increase in power flow if DLR were implemented in the region. This results in the West of John Day flow gate lines being able to transfer and additional 606 MWh. However, there is not a straightforward assessment to turn the additional capacity into an economic impact. For example, additional capacity could mean that further expansion of renewable generation is possible. It also could allow for congestion relief when line loading is high but should not be considered when loading is low.

Table. 1. Flow gate transmission lines increased capacity with DLR over a 2-year period.

Flow Gate	Lines	Static Capacity (MWh)	Dynamic Capacity (MWh)*	Increased Capacity (MWh)	Increased Capacity (%)
West of John Day	JDAY-BIGE-1	1,776	1,981	205	11.5
	JDAY-BIGE-2	1,776	1,981	205	11.5
	JDAY-MARN	1,776	1,972	196	11.0
Rock Creek Wind	RKCR-JDAY	1,361	1,488	127	9.3
John Day Wind	BIGC-JDAY	626	724	98	15.7
	KLNP-JDAY	626	766	140	22.4
West of McNary	MCNY-JDAY-2	3,552	3,900	348	9.8

* The average value over the two-year period is used for dynamic capacity

Therefore, the economic analysis only considers times when the flow gate power flow is in the highest 10% over the two-years, i.e., the time where additional capacity is useful. The top 10% of data is highlighted for John Day Wind and West of McNary in Figure 23. The increased capacity during this time and the BPA public rate of 35.56 $/MWh of electricity is then used to give an economic increase in dollars per year. The results are tabulated in Table 2.

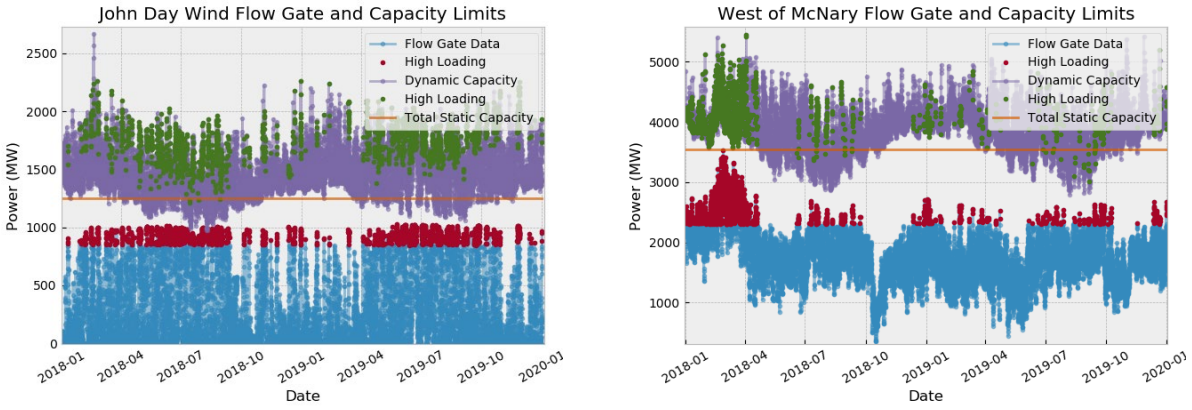

Figure 23. The (a) John Day Wind flow gate data and (b) West of McNary flow gate data with DLR capacity highlighting the top 10% of loading over a 2-year period.

Table 2. Economic impact based on highest 10% of flow gate loading.

Flow Gate	Static Capacity (MWh)	Dynamic Capacity (MWh)	Increased Capacity (MWh)	Economic Increase ($M/yr)
West of John Day	5,328	6,213	885 (16.6%)	27.58
Rock Creek Wind	1,361	1,575	214 (15.7%)	6.67
John Day Wind	1,252	1,737	485 (38.7%)	15.11
West of McNary	3,552	4,098	546 (15.4%)	16.99

4.3 New York Long Island

The weather data for the reason is plotted as wind roses in Figure 24. This is only a small sample of the 70 total weather stations across the island that had data gathered for doing the DLR calculation. Unlike the Columbia River Gorge region, the region here is a lot less sparse in terms of weather stations in the MesoWest database. The selected wind roses correspond to one at the west end at JFK airport shown in Figure 24a and the HRRR point in 24b, one near the center of the island at Mac Arthur airport shown in Figure 24c and the corresponding HRRR location in 25d, and one on the east end of the island at Gabreski airport in Figure 24e. The trend for JFK and Mac Arthur data show overall agreement with the wind direction, but the HRRR data underpredicts the local wind speeds. The data for the Gabreski airport has better speed and agreement, but directional data has more error.

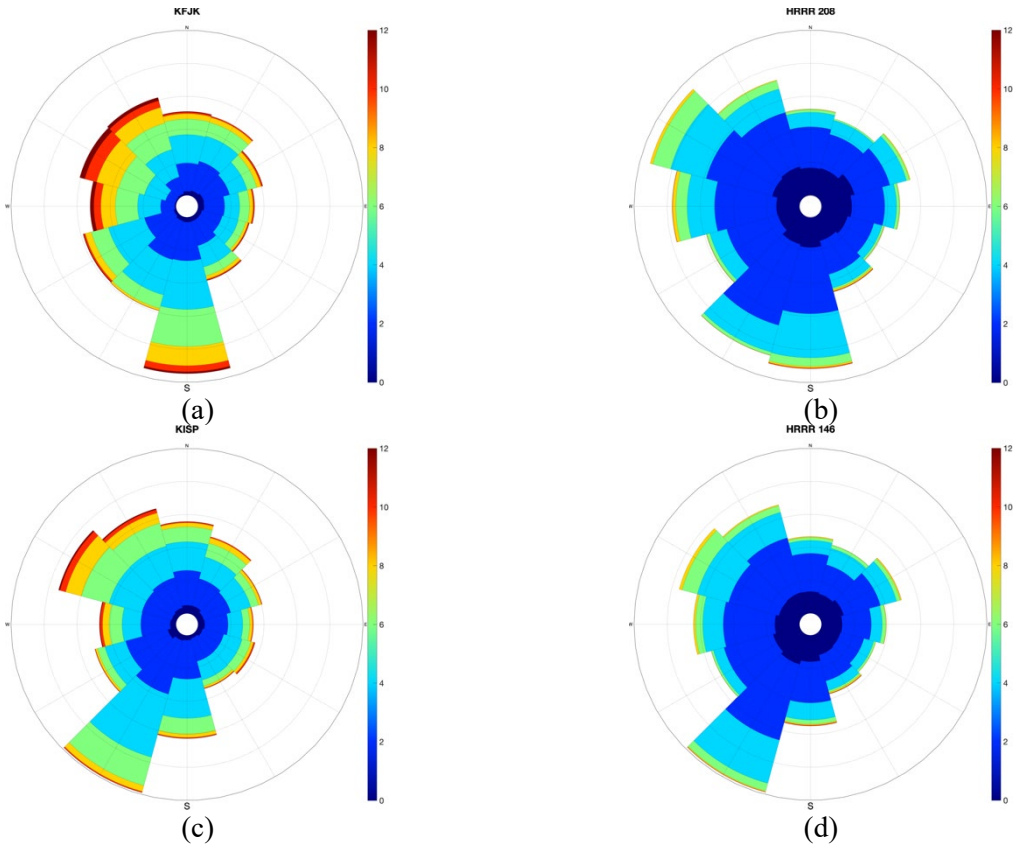

(a) (b)

(c) (d)

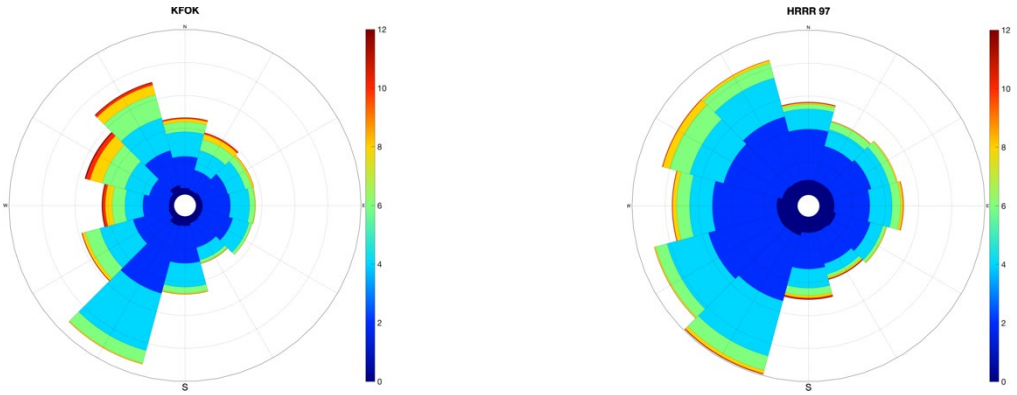

(e) (f)

Figure 24. Comparison of wind rose data on Long Island for (a) JFK airport and (b) HRRR data, (b) Mac Arthur airport (c) and (d) HRRR data, and (e) Gabreski airport and (f) HRRR data.

The wind speeds for the northern incoming sector for the wind are shown in Figure 25 for the four domains for the island. The figures go from west to east for 25a to 25d. The exterior of the island exhibits higher wind speeds than the interior of the island, mostly due to the effects of the roughness layer modeled from the suburban/urban terrain, as elevation changes are minor.

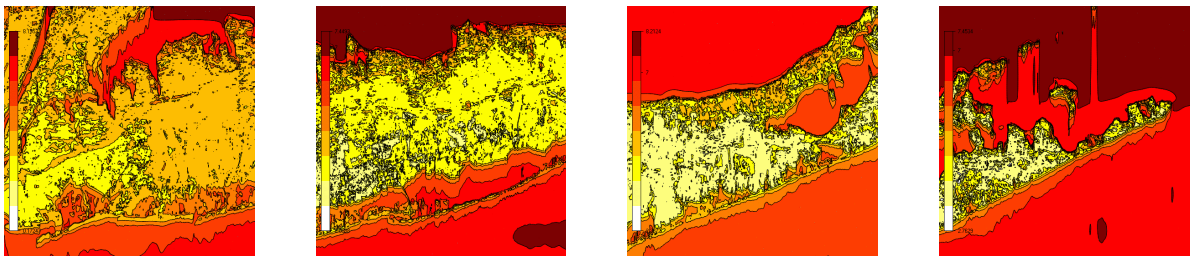

(a) (b) (c) (d)

Figure 25. CFD modeling of the domain decomposition of Long Island from northern incoming wind. The legend range is approximately 0-8.0 m/s.

The wind plants are modeled with both the weather station transferred data, and with the forecasted data from the HRRR model points. The histogram of this data over 3 years is shown in Figure 26. In general, the data shows that the wind power production from the weather station transfers is biased towards zero or maximum production much more so than the forecasted data predictions. Of note though, is that the nearest weather stations to the offshore wind plants are 10s of kilometers away, so some bias of the observation data may exist here that should be studied in the future. With access to offshore wind buoy or other meteorological wind data closer to the wind plant sites, these resulting observational prediction could be improved.

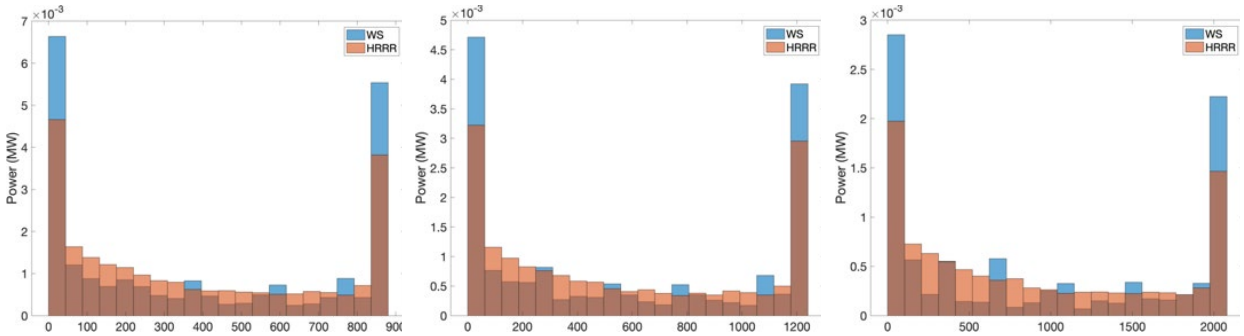

Figure 26. Wind power histograms for (a) Sunrise, (b) Beacon and (c) Empire wind plants.

Buoy information was also studied, and it was examined to bring in data from source in the New York Bight from NYSERDA, buoys, installed from the PNNL project, and buoys from NOAA's national database buoy center. The comparison of the wind plants with the buoy data is shown in Figure 27, Overall, this improves the accuracy of the HRRR to weather observation comparison across all three modeled wind farms for the central part of the curve but some the frequency of zero power generation is underpredicted.

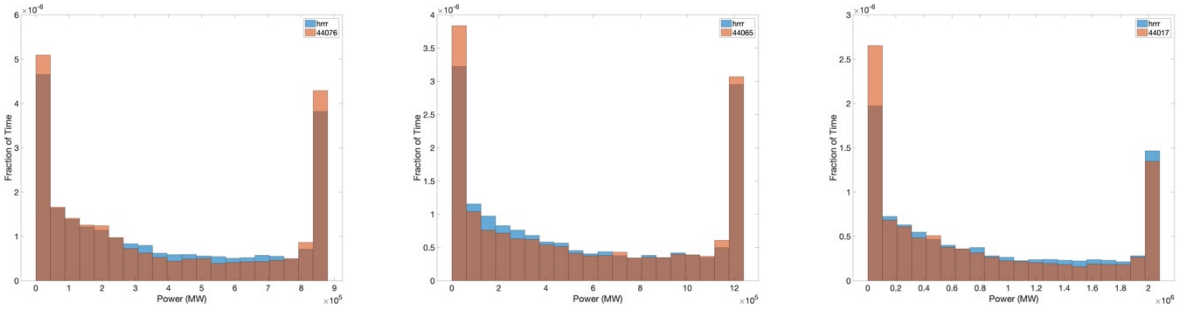

Figure 27. Wind power histograms for (a) Sunrise, (b) Beacon and (c) Empire wind plants with buoy weather data.

The ampacity for the two line segments for both the observational DLR ratings and the HRRR forecasted ratings are shown for the time period in Figure 28a. The winter periods have very high spikes in the ampacity correlating with high wind occurrences. The shorter Line 1 pathway has a higher average ampacity than that of the longer line 2 pathway; 1127 A compared to 1074 A for a Drake conductor. The histogram of the availability of the additional ampacity over static is shown in Figure 28b compared to both parallel and perpendicular static ratings. Line 1 has additional capacity above a perpendicular rating about 20% of the time, while this is negligible for Line 2, in addition Line 1 is above a parallel static rating all the time, while Line 2 shows some brief time periods below parallel static.

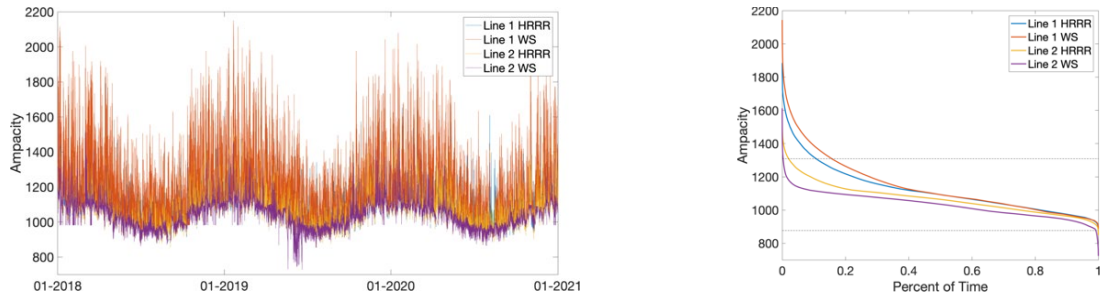

(a) (b)

Figure 28. The (a) raw ampacity for both transmission pathways and (b) plot of ampacity availability over static rating for both observational and forecasted DLR.

The error of the forecast data for the two lines is shown in Figure 29a for the short transmission line and in Figure 29b for the long transmission line. With error of the observational DLR compared to the forecasted ampacities, the shorter Line 1 pathway has an average error of 89 A, and the longer Line 2 pathway has an average error of 47 A, for 8.8% and 4.7 %, respectively. The low error is likely due to the lower overall ampacity on the longer line. With more weather stations deployed this takes the minimum across all of them likening the possibility that both a HRRR data point and a weather station data point utilize a low wind speed simultaneously even though the overall wind roses may not match as well as other regions.

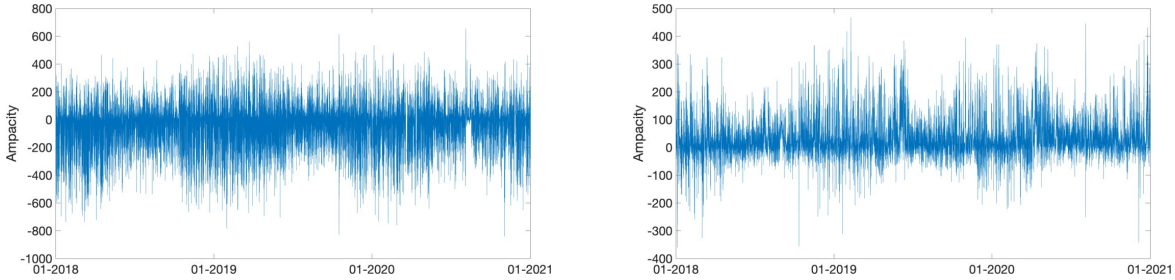

(a) (b)

Figure 29. The forecasted minus observed ampacity for the (a) short regional line and the (b) long regional line.

Figure 30a shows both the power generation and the observed DLR ampacity for the line connection the Empire wind plant to the grid, the short line, and Figure 30b shows the generation and ampacity for the line connecting Sunrise and Beacon, the long line. Several months of data were cropped from the short line comparison as the buoy was offline for a period of time. As with the INL site data, since no load data is available, a normalization to both variables is used, with the same 20% above static assumption for the ampacity. Given the large power load for the offshore wind project compared to the INL wind farm, the 20% may be insufficient, but this keeps the comparison simple. With the normalized variable anytime it dips below 1, then the rating is less than 120% of the static. The normalized variables are plotted in Figure 31a and 31b for the full time period, for the short and long lines, from which is becomes hard to discern the effect. The normalized variables are plotted in small time frame segments in Figures 32a-c for the short ling and for Figures 32d-f for the long line. The shorter line off maintains levels of its DLR rating well above 1 when the wind power generation is peaked, pointing to long periods where the concurrent cooling effect is valid for the line. The longer line shows this effect much less frequently and in some of the dates plotted the normalized ampacity dips below 1 when the wind power is

peaked, which is a case that could require curtailment of the power generation. Notably in 32e the ampacity is quite low pointing to a large period with low wind on the large, yet the offshore wind is quite high. The effects need to be studied for deployment of DLR solutions of offshore wind over long-distance lines.

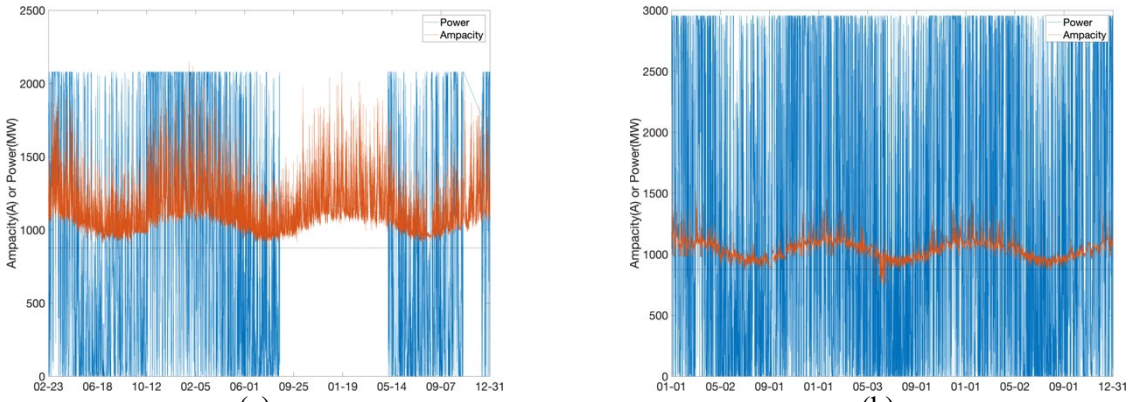

(a) (b)

Figure 30. The wind power generation and ampacity for the (a) short transmission line and the (b) long transmission line.

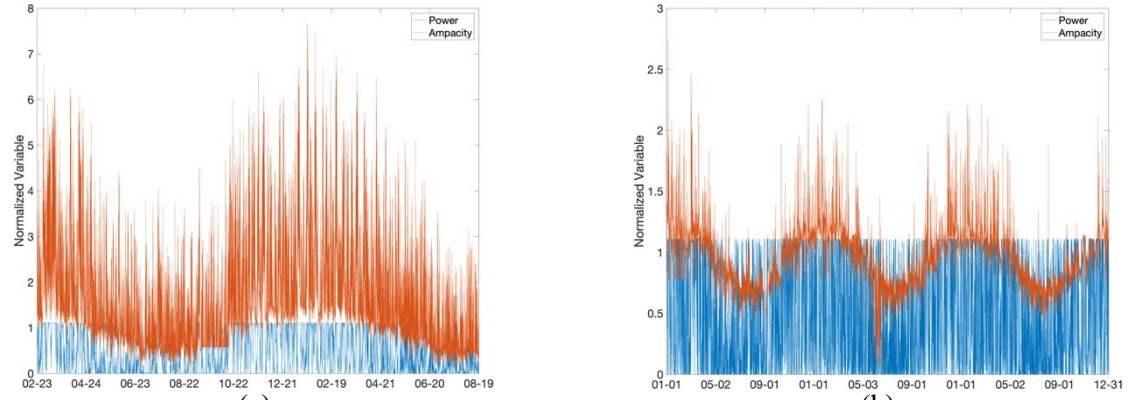

(a) (b)

Figure 31. The normalized wind power generation and ampacity for the (a) short transmission line and the (b) long transmission line.

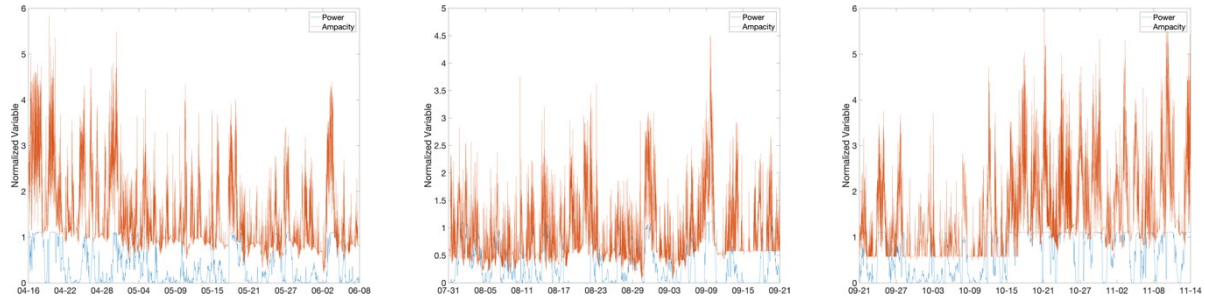

(a) (b) (c)

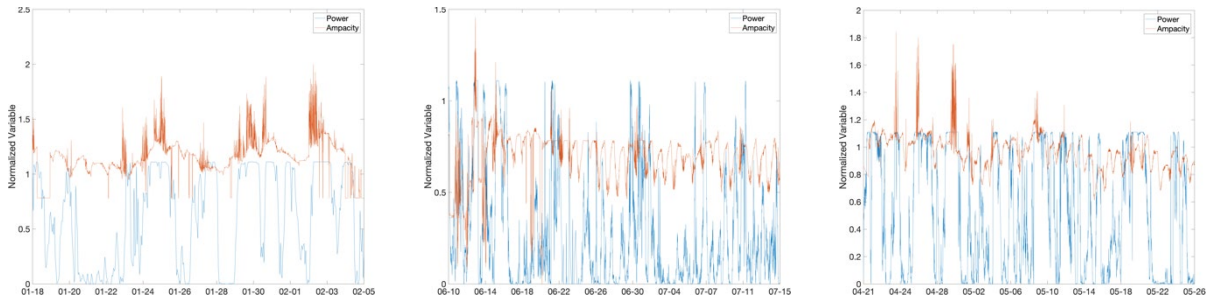

(d) (e) (f)

Figure 32. The wind power generation and ampacity for the (a-c) short transmission line and the (d-f) long transmission line for selected periods.

The normalized wind power is then subtracted from the normalized ampacity, and values below zero point to time periods where curtailment may be needed. This data is then tabulated into a CDF function with the 120% static normalization for the two lines. The CDF for the short line is shown in Figure 33a. As with the short line modeled in Idaho the value of this function is right at 0.07 for the fraction of time that curtailment could be needed, so there is a high correlation for the concurrent cooling effect for this line. However, for the longer line shown in Figure 33b, this value increased by a factor of 2 to about 0.15 for the fraction of time that curtailment could be needed due to peak wind generation offshore not coinciding with high winds near the transmission lines. This is also repeated for a normalization of 10% above static for the two lines, this is shown in Figure 33c and Figure 33d. Here the fraction of time that could require curtailment drops to 1% and 3% for the short and the long lines, respectively.

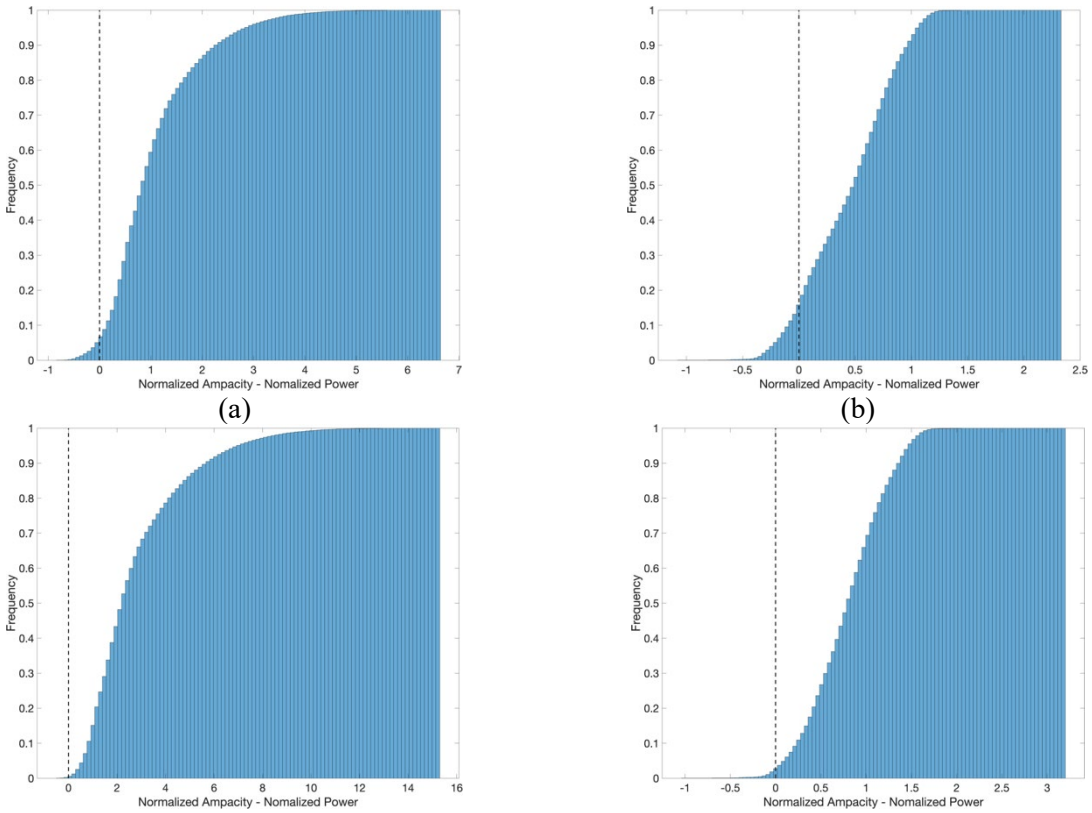

(a) (b) (c) (d)

Figure 33. The CDF for normalized ampacity – normalized power generation for (a) short transmission line and (b) long transmission line. The CDF for normalized 110% ampacity – normalized power generation for (a) short transmission line and (b) long transmission line.

5. Conclusions

A selection of wind plants across Idaho, the Columbia River Gorge and offshore wind in the NYSERDA territory were modeled for their concurrent cooling effects for dynamic line rating. Regional transmission lines for the wind plant interconnections were determined and a CFD domain was created to determine local wind flows over the lines. A dynamic line rating for each of the lines was calculated for both weather observation data and HRRR model forecast data. The comparison of peaks in the wind power production were compared to the DLR peaks.

It was determined that for shorter regional transmission lines, the effect of concurrent cooling that commonly occur with gen-tie lines were still valid. Concurrent cooling effects drop as the length of the regional transmission lines increase in distance from the wind plants. In addition, the accuracy of the forecasted ampacity to the weather observation data for ampacity was assessed. In general, the accuracy was dependent on having local weather stations, as the New York and INL data sets both showed higher levels of accuracy than the Columbia Gorge and its sparse arrangement of weather stations.

REFERENCES

Alexander W. Abboud, Kenneth R. Fenton, Jacob P. Lehmer, Benjamin A. Fehringer, Jake P. Gentle, Timothy R. McJunkin, Katya L. Le Blanc, Melissa A. Petty, and Matthew S. Wandishin. "Coupling computational fluid dynamics with the high resolution rapid refresh model for forecasting dynamic line ratings." *Electric Power Systems Research* 170 (2019a): 326-337.

Alexander W. Abboud, Jake P. Gentle, Timothy R. McJunkin, and Jacob P. Lehmer. "Using Computational Fluid Dynamics of Wind Simulations Coupled with Weather Data to Calculate Dynamic Line Ratings." *IEEE Transactions on Power Delivery* 35, no. 2 (2019b): 745-753.

Alexander Abboud, Jacob Lehmer, and Jake Gentle. “Concurrent Cooling Effects of Dynamic Line Ratings on Wind Plant Gen-Tie Lines.” Idaho National Laboratory, Tech. Rep. INL-RPT-22-66031. 2022.

J. Ahmad, A. Malik, L. Xia, N. Ashikin,"Vegetation encroachment monitoring for transmission lines right-of-ways: A survey,”, Electric Power Systems Research, Volume 95, 2013, pp 339-352.

B. J. L. Aznarte and N. Siebert, “Dynamic line rating using numerical weather predictions and machine learning: A case study,” IEEE Trans. Power Delivery, vol. 32, no. 1, pp. 335–343, 2017.

B. Banerjee, D. Jayaweera, S. Islam. “Risk constrained short-term scheduling with dynamic line ratings for increased penetration of wind power.” Renew Energy, 83 (2015), pp. 1139-1146.

S. G. Benjamin, S. S. Weygandt, J. M. Brown, M. Hu, C. R. Alexander, T. G. Smirnova, J. B. Olson, E. P. James, D. C. Dowell, G. A. Grell, et al., A north American hourly assimilation and model forecast cycle: The rapid refresh, Mon. Weather Rev. 144 (2016) 1669–1694.

B. P. Bhattarai, J. P. Gentle, P. Hill, T. McJunkin, K. S. Myers, A. Abboud, R. Renwick, and D. Hengst, “Trans- mission line ampacity improvements of altalink wind plant overhead tie-lines using weather-based dynamic line ratings,” in IEEE PES General Meeting, July 2017.

B. P. Bhattarai, J. P. Gentle, T. McJunkin, P. J. Hill, K. Myers, A. Abboud, and D. Hengst, "Improvement of transmission line ampacity utilization by weather-based dynamic line ratings," IEEE Transactions on Power Delivery, 33(4), pp 1853-1863.

J. Cao, W. Du, H.F. Wang. "Weather-based optimal power flow with wind farms integration." IEEE Trans Power Syst, 31 (4) (2016), pp. 3073-3081

CIGRE Working Group 22.12, "The thermal behaviour of overhead line conductors," Electra, vol. 114, no. 3, pp. 107–125, 1992.

"Guide for selection of weather parameters for bare overhead conductor ratings," CIGRE WG 22.12, Tech. Rep., 2006.

"Guide for thermal rating calculations of overhead lines," CIGRE WG B2.43, Tech. Rep., 2014.

E.W. Dijkstra, A note on two problems in connection with graphs, Numer. Math. l (1959) 269–271.

D. Greenwood, J. Gentle, K. Myers, P. Davison, I. West, J. Bush, G. Ingram, and M. Troffaes, "A comparison of real-time thermal rating systems in the U.S. and the U.K." IEEE Trans. Power Delivery, vol. 29, no. 4, pp. 1849– 1858, August 2014.

IEA (2021), Renewable Energy Market Update 2021, IEA, Paris https://www.iea.org/reports/renewable-energy-market-update-2021

"Overhead electrical conductors calculation methods for stranded bare conductors," IEC Standard TR 1597, Tech. Rep., 1985.

"Standard for calculating current-temperature relationship of bare overhead line conductors," IEEE Standard 738, Tech. Rep., 2012.

IEEE PES WG Subcommittee 15.11, "Real-time over- head transmission line monitoring for dynamic rating," IEEE Transactions on Power Delivery, vol. 31, no. 3, 2016.

W. Jones and B. Launder, "The prediction of laminarization with a two-equation model of turbulence," International journal of heat and mass transfer, vol. 15, no. 2, pp. 301–314, 1972.

Southwire Company, Product Database and Specifications, https://www.southwire.com/wire-cable/bare-aluminum-overhead-transmission-distribution/c/c-bare-aluminum-overhead

T. Smith, S. Benjamin, J. Brown, S. Weygandt, T. Smirnova, B. Schwartz, Convection forecasts from the hourly updated, 3-km high resolution rapid refresh (hrrr) model., in: 24th Conference on Severe Local Storms, Savanah, GA, 2008.

S. Talpur, C.J. Wallnerstrom, C. Flood, P. Hilber. "Implementation of dynamic line rating in a sub-transmission system for wind power integration." Smart Grid Renew Energy, 6 (8) (2015), pp. 233-249

I. Toren and E. L. Petersen, European Wind Atlas. Risø National Laboratory, 1989.

"Dynamic line rating systems for transmission lines: American recovery and reinvestment act of 2009," U.S. Department of Energy, Tech. Rep., 2014.

"Smart grid system report," U.S. Department of Energy, Tech. Rep., 2010.

S. Uski-Joutsenvuo and R. Pasonen, "Maximizing power line transmission capability by employing dynamic line ratings technical survey and applicability in finland, vtt- r-01604-13," Tech. Rep., 2013.